An accurate closure for the configuration dynamics and rheology of dilute polymer chains in arbitrary flows

Indranil Saha Dalal[1], Praphul Kumar[1] and Ronald G. Larson[2*]

[1]Department of Chemical Engineering, IIT Kanpur, Kanpur, India.

[2]Department of Chemical Engineering, University of Michigan Ann Arbor, USA.

*Corresponding author

For Table of Contents use only

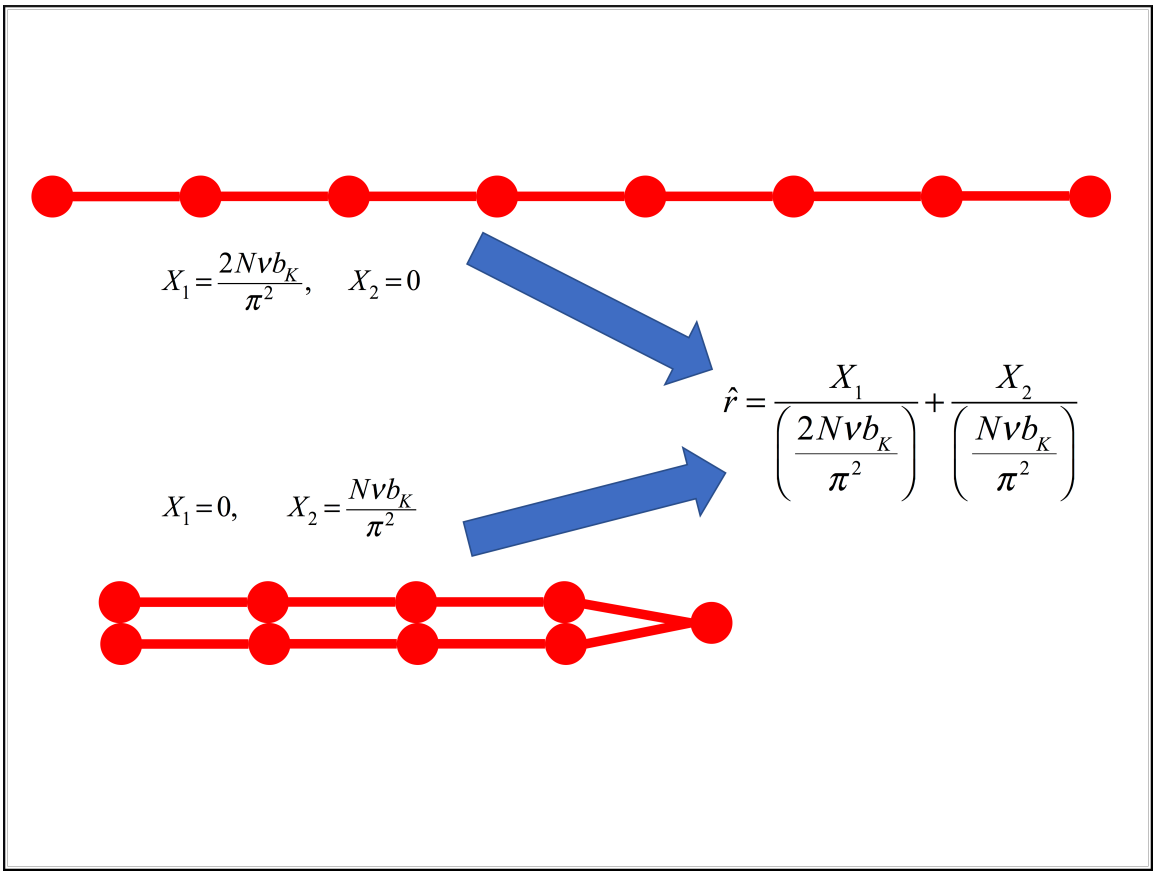

Abstract:

We present a new, "FENE-mode", constitutive model for conformation and stress dynamics of dilute polymer chains in arbitrary flows, obtained by pre-averaging equations for the normal modes using a "representative" spring constant that depends on the magnitudes of both the first and second modes, accounting for both overall chain stretch and chain folds. Simulations with this model are orders of magnitude faster than with multi-spring Brownian dynamics (BD) simulations, and yet retain more of their accuracy than other pre-averaged models. This is demonstrated by comparing the predictions of the FENE-mode model with those from BD simulations in start-up of uniaxial extension, steady shear, and mixed flows. For all cases, we find that, even when few modes are used, the transient and final steady-state conformations and stresses are in much better agreement with BD predictions than those of the existing pre-averaged FENE-P and the FENE-PM models. The possibility of extension of the approach to the more important case of entangled polymers is also discussed. Because the model allows cost-accuracy trade-offs to be made through choice of the number of modes used, the model should be ideal for multi-dimensional simulations of polymer flows.

Introduction:

The dynamics of dilute polymer solutions have been thoroughly investigated over the last few decades by various experimental and theoretical techniques under equilibrium (no-flow) and flowing conditions [1-11]. The experimental studies include rheological measurements, light scattering and, more recently, fluorescent microscopy of DNA chains that serve as model polymer chains. The studies under no-flow conditions have yielded chain dimensions and segmental dynamics that can be compared with analytical models. Under flow, the primary interest is in

determining the deformations of the ensemble of chains accurately enough to compute the corresponding stresses and flow field with suitable accuracy. Ideally, one derives a constitutive equation that, when combined with the momentum balance equations, yields the velocity and stress fields, as well as the other quantities, such as chain orientation, that are of engineering interest.

Researchers have used a variety of methods to understand the physics of chain dynamics under the influence of flow, the most detailed of which is DNA imaging [1-4, 8]. Theoretical models have been inspired by the seminal work of Rouse [12], who described the chain dynamics through the introduction of normal modes. The effect of hydrodynamic interactions (HI) was incorporated later by Zimm in the linear viscoelastic regime [13], which yielded results that agreed well with experimental measurements. The framework set by the Rouse and Zimm models was closely followed by computational techniques, which also modeled the polymer chain by beads connected by springs. While only a few beads and springs [14-22] and dumbbells [49-50] were used in the early days when computational power was limited, in recent years the phenomenal rise in computer power has allowed analysis of highly detailed models that retain hundreds or thousands of degrees of freedom using Brownian dynamics (BD) or molecular dynamics (MD) simulations [23-27, 44-45]. A summary of the findings of earlier work is given in various review articles [28, 41-43]. Most of those investigations were restricted to extensional and shear flows, while a few have explored planar mixed flows ranging between extensional to purely rotational [20]. In a fast extensional flow, the chain attains a nearly completely extended final state while in a fast shearing flow, which contains equal amounts of extension and rotation, the long-time behavior consists of incessant end-over-end tumbling events. Thus, in a shearing flow, the average chain stretch plateaus at a value equal to around half of the contour length at high shear rates. A few earlier

observations also reported chain compression, or shrinkage of the chain dimension, relative to equilibrium, at very high shear rates [23]. However, recent Brownian dynamics simulations have revealed those to be artifacts of inadequate chain discretization, which must be made finer with increasing shear rate to avoid spurious chain collapse [24]. The dynamics in planar mixed flows have been found to be a combination of stretching and tumbling [20]. Further detailed investigations of mixed flows can be found in some recent studies [46-47].

Brownian dynamics simulations, in which the polymer chain is modeled by a set of beads and springs, have proven to be highly successful in describing the temporal evolution of chain conformations. However, to arrive at the ensemble average of any time-dependent quantity from Brownian dynamics simulations, one needs to simulate a large number of chains with different initial configurations. This results in a very high computational cost for three-dimensional flow simulations, even when the polymer chain is mimicked by modest numbers of springs. A purely analytical ensemble-averaged constitutive model for multiple beads and springs, if available, would be extremely valuable in reducing this cost. Several such one-mode models for dilute polymer solutions have been developed, including the "FENE-P" and "FENE-PM" models by Bird and coworkers, which, however, lack the desired accuracy in mimicking the time evolution observed in BD simulations, particularly in shear flows [29]. Much more recently, Ghosh and coworkers formulated the adaptive length scale (ALS) model [30]. However, much like the previous models, the performance in shear flow was largely similar to that of the FENE-P model. One can gain improved accuracy by expanding these models to multi-mode versions, allowing the linear rheological behavior to be predicted with high accuracy when many modes are used. However, in the nonlinear state, both single-mode and multi-mode models must employ closure

approximation such as pre-averaging or Gaussian averaging to cope with the nonlinearity of the spring constant. In doing so, one is confronted with "molecular individualism" in which, at high strain rates, different chains in the ensemble possess very different states of stretch and hence different spring constants. In particular, high rates of strain yield various partially folded states, in which chains that are far from being fully extended, nevertheless, because of their high local stretch, exhibit high spring constants characteristic of the fully extended chain. While folded chain configurations in extensional flow converge at high extension rate to nearly fully extended states [2], in shear, even at steady state, the ensemble contains chains at various states of unraveling and collapsing back into internally folded chains [1]. As we discuss below, simple pre-averaging of the spring constant based on the overall stretch of the whole molecule fails to account for the effect of internal folds. Such pre-averaging schemes only reflect the influence of the slowest polymer mode on the spring constant, while in general all modes affect the spring constant, and each mode has its own effective spring constant. Capturing these effects within a constitutive equation is rather complex, but the consistent averaging technique by Öttinger and coworkers [31] of doing so has been promising. More recently, a sophisticated Gaussian averaging method by Prabhakar and Prakash [32] has shown success in capturing not only the effects of finite extensibility but also of hydrodynamic interactions. Kishbaugh and McHugh [48] have also derived approximate normal mode equations for bead-spring chain models with non-linear springs and hydrodynamic interactions.

Here, to cope with this issue in a simpler, and more efficient, way, we formulate a new multi-mode constitutive model for chains with multiple beads and springs that, by using a "representative" spring constant that is a simple linear combination of the magnitudes of the first and second modes,

can predict the results of detailed BD simulations with surprisingly high accuracy in extensional, shear, and mixed flows, indicating its applicability to any general flow. If the normal modes are known at any instant, the chain conformational properties (and the corresponding stress) can be easily computed. We show here that our new "Fene-mode" model is able to reproduce the average temporal evolution of chain dynamics of the full BD simulations in both extensional and shear flows, as well as in other planar mixed flows that range from purely extensional to purely rotational. Since the stresses are also predicted fairly accurately, this model can potentially be coupled with CFD solvers to predict multi-dimensional viscoelastic flow fields and stresses. To illustrate the potential for this, we provide here a comparison of some predictions from our model and of the FENE-P (developed by Bird and coworkers [33] and incorporated into CFD packages like ANSYS POLYFLOW and COMSOL) that clearly highlights the superiority of our model in reproducing the temporal evolution of stresses, especially in shear flow. We also compare the speed and accuracy of the Fene-mode model with that of multi-mode preaveraged models. Since theories for entangled polymers often involve decomposition of stress into a product of a chain orientation tensor and a chain stretch prefactor [34], we hope that our development of a method of handling chain stretch more accurately might also be applied to entangled solutions.

Methods and model:

Brownian dynamics (BD) simulations:

The BD simulations performed in this work follow the algorithms and equations described in previous work [24], and we only provide a brief discussion here. The polymer chain is represented by $N + 1$ beads (numbered 0 to N) that are connected by N (numbered 1 to N) springs. Note, the effects of excluded volume and hydrodynamic interactions are beyond the scope of this work.

These will be incorporated in a future study. The equation of motion of any bead is therefore given as:

$$\frac{d\vec{r}_i}{dt} = \frac{1}{\zeta}\vec{F}_i^{\,flow} + \frac{1}{\zeta}\left[\vec{F}_{i+1}^{\,S} - \vec{F}_i^{\,S}\right] + \frac{1}{\zeta}\vec{F}_i^{\,R} \tag{1}$$

where ζ is the drag coefficient, $\vec{r}_i$ is the position vector of the i^{th} bead, $\vec{F}_i^{\,R}$ is the Brownian force on the i^{th} bead, $\vec{F}_i^{\,flow}$ is the force on the bead due to the flow field, and $\vec{F}_i^{\,S}$ and $\vec{F}_{i+1}^{\,S}$ represent the forces exerted due to the i^{th} and $(i+1)^{th}$ springs, respectively. Here, the force due to flow is given as:

$$\vec{F}_i^{\,flow} = \zeta\hat{\kappa}\cdot\vec{r}_i \tag{2}$$

where the tensor $\hat{\kappa}$ is given as:

$$\hat{\kappa} = \left(\nabla\vec{\mathrm{v}}\right)^T \tag{3}$$

where $\vec{\mathrm{v}}$ is the velocity field and ∇ is the gradient operator. The Brownian force on the i^{th} bead is given by $\sqrt{\mathrm{k_B T}\zeta}\,d\vec{W}$, where $d\vec{W}$ represents a Wiener process in three dimensions. For the implementation of the same in BD simulations, we used the following form in our algorithm [24]:

$$\vec{F}_i^{\,R} = \sqrt{\frac{6\mathrm{k_B T}\zeta}{\Delta t}}\,\vec{n}_i \tag{4}$$

where T is the absolute temperature, $\mathrm{k_B}$ is the Boltzmann constant and $\vec{n}_i$ is a vector whose components are uniformly distributed within the interval [-1, 1]. We perform BD simulations using the dimensionless forms of these equations given here. The procedure to obtain the non-dimensional form is discussed in detail in the earlier study [24].

In this work, most of the simulations are performed using bead-spring models for polymer chains with spring forces given by the Cohen-Padé approximation:

$$\frac{F^S b_K}{\mathrm{k_B T}} = \frac{\alpha \hat{r} - \beta \hat{r}^3}{1 - \hat{r}^2} \tag{5}$$

where $\hat{r}$ denotes the fractional spring extension, relative to the fully extended length, and $\alpha = 3$ and $\beta = 1$. For comparison, a few simulations are performed using stiff Fraenkel springs, where the spring forces are given by:

$$\vec{F} = K_F \left(\left| \vec{Q} \right| - b_K \right) \frac{\vec{Q}}{\left| \vec{Q} \right|} \tag{6}$$

where $\vec{Q}$ represents the spring vector, b_K is the length of the Kuhn step and K_F is the spring constant. A high value of the Fraenkel spring constant creates a stiff spring, which mimics a rod [24-25].

Now, we derive the equations needed to model the temporal evolution of the chain configuration for various types of flow fields. As discussed in the next few sections, we obtain simplified equations for the evolution of the modes of a polymer chain, using a "representative" spring constant for the chain that also evolves with time, as set by the magnitudes of the two slowest modes.

Temporal Evolution of modes

In our model, the dynamics of the polymer chain are analyzed through the temporal evolution of the normal modes. For a polymer chain of N springs or (N+1) beads, numbered 0 to N, the p^{th} normal mode is defined as [35]:

$$\vec{X}_p(t) = \frac{1}{N}\int_0^N dn \cos\left(\frac{p\pi n}{N}\right)\vec{r}_n(t) \tag{7}$$

where the position vectors of the beads are given as $\vec{r}_n$. The temporal evolution of the correlations of the components of the normal modes in any flow field is given by [35]:

$$\frac{d}{dt}\left\langle \vec{X}_p \vec{X}_p \right\rangle = \frac{1}{\zeta_p}\left[2k_B T\underline{\underline{\delta}} - 2k_p\left\langle \vec{X}_p \vec{X}_p \right\rangle\right] + \hat{\kappa}\bullet\left\langle \vec{X}_p \vec{X}_p \right\rangle + \left\langle \vec{X}_p \vec{X}_p \right\rangle \bullet \hat{\kappa}^T \tag{8}$$

Note that, to arrive at Eq. (8), the spring constant k has been assumed to be same for all springs. Here, $k_p = 2\pi^2 kp^2/N$, where, at equilibrium, the spring constant is given as $k_{eq} = H = 3\mathrm{k_B T}/\nu b_K^{\ 2}$ (H is the entropic linear spring constant). Also, k_B is the Boltzmann constant, T is the temperature, ν is the number of Kuhn steps mimicked by a single spring of the bead-spring model, and b_K is the length of one Kuhn step. In Eq. (8), $\zeta_p = 2N\zeta$ (as defined in the text by Doi and Edwards [35]), where ζ is the bead drag coefficient mentioned earlier. The tensor $\hat{\kappa}$ is defined by Eq. (3).

One can integrate Eq. (8) numerically to obtain the temporal evolution of the normal modes for any general flow field. However, in this article, we primarily consider standard shear and extensional flows (and some planar mixed flows), for which one could obtain analytical solutions for the evolution of the normal modes, if the spring constant and drag coefficient are constant. Since we will here consider cases in which the spring constant evolves with time, we cannot obtain fully analytical solutions. However, we can integrate analytically the differential mode equations over a small time interval over which the spring constant does not change significantly. This yields difference equations that can be solved numerically, allowing the spring constant to vary from one time step to the next, to obtain the evolution of various correlations, including those needed to

compute stress. (Note that numerical integration of the general equation, Eq. (8), is necessary for complicated flow fields that don't yield simple analytical solutions.) These analytical normal mode difference equations for the flow fields used in this study are provided in the appendix. It can also be shown that these solutions satisfy the differential equation for the evolution of the correlations of the components of the normal modes (given by Eq. (8)).

Spring constant:

The above solutions are exactly those of the well-known Rouse theory (with the addition of flow fields), as long as the spring constant k is in fact constant, implying Hookean (i.e., linear) springs. However, since the polymer chains are exposed to the flow field, the springs (and the entire chain) are deformed from their equilibrium lengths and for realistic, finitely extensible springs, the force-stretch behavior of the spring becomes nonlinear. At any given time during deformation, we therefore denote the instantaneous spring constant as $k = Hf$, where f represents the ratio of the value of the spring constant to its value at equilibrium (i.e. H), which we pre-average over the distribution of spring conformations at each instant in time. If we were working with a single spring, or dumbbell model, our approach would be identical to that used to develop the "FENE-P" or pre-averaged FENE dumbell model. However, the FENE dumbbell model leads to relatively inaccurate predictions of stresses in shear flow and in transient stresses in start-up of extensional flow, because of its neglect of internal polymer conformations that are only captured by using multiple springs per molecule. In what follows, we retain use of a single pre-averaged spring constant that is the same for every spring, as well as the use of normal modes, but apply this to a polymer represented by multiple springs. The task then is to provide a simple approximate relationship connecting this spring nonlinearity f to the magnitudes of the modal variables of the

chain. Henceforth, the square root of $\left(\left\langle X_{px}^2 \right\rangle + \left\langle X_{py}^2 \right\rangle + \left\langle X_{pz}^2 \right\rangle\right)$ is referred to as the magnitude of the pth mode and denoted by $\bar{X}_p$ in this manuscript.

Our approach is to express the effective spring constant (also called the "representative spring constant") as a function of the overall state of stretch in the chain. Note here, for a purely stretching flow (i.e. extensional flow) without any rotation, the chain stretches out without any tumbling [2, 21]. Thus, the chain can be approximated as a stretched object with a few folds, although for long chains in very fast flows, there is a stage of multiply-folded states through which the chain passes (an example of such a temporary folded state is shown in Figure 1(a)) . In shear flow, it is well established that chains undergo an incessant end-over-end tumbling even when the behavior of the ensemble reaches steady state [8, 24-25]. For strong shear flows, this tumbling process is observed even when the chain is in a highly stretched state. This is in contrast to extensional flows, where the end-over-end tumbling, initiated at the chain end through folds, is absent. An end-over-end tumbling event, initiated at one chain end through a fold, is shown in Figure 1(b).

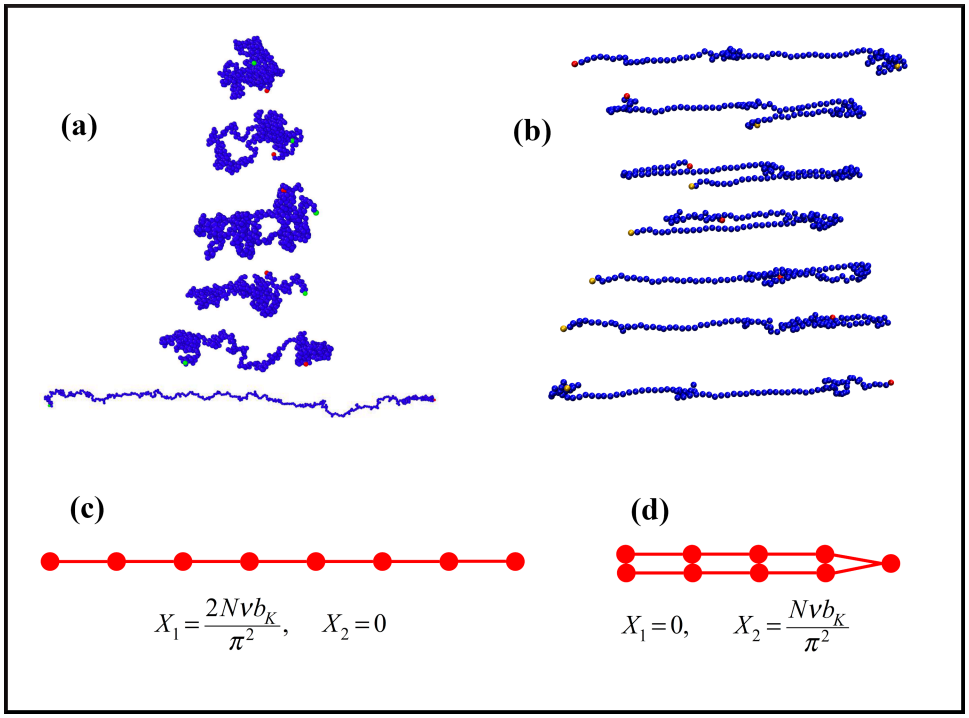

Figure 1: (a) Example of temporary folded states through which a chain evolves to a stretched state in strong extensional flow, (b) an end-over-end tumbling event of a polymer chain in strong shear flow, initiated by a fold at an end, (c) schematic of the fully stretched state of the polymer chain, where the magnitudes of the first and second modes reach a maximum and minimum (zero), respectively and (d) a schematic of a hairpin-like fold when the second mode attains a maximum value, but first mode vanishes. The respective magnitudes are indicated in (c) and (d).

Thus, to estimate the effective spring constant in an extensional flow, we only need a measure of the state of stretch of the chain relative to the maximum stretch that can be attained. In this context, we note that the root-mean-square magnitude of first mode, $\overline{X}_1$, attains a maximum value of $\frac{2Nvb_K}{\pi^2}$ when the chain is fully stretched, while the corresponding magnitude of the second mode $\overline{X}_2$ vanishes for a fully stretched chain (a schematic is shown in Figure 1(c)). Thus, from this

observation, we can obtain the ensemble average end-to-end length of the chain at any time in the later stages of extensional flow from the value of the first mode at that time, relative to its maximum value. This implies that for chains that are nearly fully stretched, f can be assumed to be a function of the normalized first mode, $\frac{\bar{X}_1}{\left(\frac{2N\nu b_K}{\pi^2}\right)}$, alone.

Shear flows and mixed flows have both stretching and rotational components, where in shear the extension and rotation are present in equal magnitudes [1]. For fast shear flows, at steady state, the chain forms folds, typically initiated at the chains ends, leading to tumbling and the formation of hairpin-like folds, with the chain nearly fully stretched every where except at the folds. These hairpin-like folds also form as transients in start-up of fast extensional flows [4]. Thus, when a locally highly stretched, folded, configuration forms, the effective spring constant should be similar to that of a chain which is globally stretched in a strong extensional flow. However, owing to the presence of folds, the end-to-end vector of the chain is much less than its maximum value and so the normalized first-mode magnitude $\frac{\bar{X}_1}{\left(\frac{2N\nu b_K}{\pi^2}\right)}$ is not close to unity. Thus, if the spring constant were to depend only on this variable, one would predict a much lower value of the spring constant. In fact, a chain that is locally almost fully stretched, but folded exactly in half, would show a zero value of $\frac{\bar{X}_1}{\left(\frac{2N\nu b_K}{\pi^2}\right)}$ since the two ends of the chain lie on top of each other. If the spring constant were to depend only on this normalized first-mode magnitude, it would not differ from its value in the absence of flow.

Thus, a dependence on other modes is required to account for the effect of these internally folded states, which occur when the polymer is locally, but not globally, highly stretched. At a minimum, then, we need to include a dependence on the magnitude of the second mode $\bar{X}_2$, normalized by its maximum value of $\frac{Nvb_K}{\pi^2}$, where the maximum value is attained when the chain is locally fully stretched, but has a hairpin fold at its center (schematic shown in Figure 1(d)). For this configuration, the first mode $\bar{X}_1$ vanishes, as mentioned above. Thus, if we wish to model the spring constant realistically for chains that can be either fully extended globally, or fully extended locally but folded in the center, the spring constant must depend, at a minimum, on the two ratios $\frac{\bar{X}_1}{\left(\frac{2Nvb_K}{\pi^2}\right)}$ and $\frac{\bar{X}_2}{\left(\frac{Nvb_K}{\pi^2}\right)}$.

Here, we use only these two modes to determine the spring constant of the chain, although we will use many modes to determine the stress. Since we are primarily using springs that follow the Cohen-Padé spring model, the effective spring constant will also be calculated using these same two modes, using an effective fractional stretch of the springs, designated here by $\hat{r}$, which we take to be a function of $\frac{\bar{X}_1}{\left(\frac{2Nvb_K}{\pi^2}\right)}$ and $\frac{\bar{X}_2}{\left(\frac{Nvb_K}{\pi^2}\right)}$. Here, we use the simplest linear function possible – a sum of the two factors with equal weighting. A simple justification of this is provided by an estimate of the state of stretch in a chain in a fast flow field, where the chain is treated as a one-dimensional object with one hairpin-like fold at one end. The chain consists of a total of N

springs, each stretched to a length l_{sp}. The fold occurs at the bead position N_f (i.e. the last $N - N_f$ springs constitute the fold). The p^{th} mode can be calculated as:

$$X_p = \left[\frac{1}{N} \int_0^{N_f} n l_{sp} \cos\left(\frac{p\pi n}{N} \right) dn \right] + \left[\frac{1}{N} \int_{N_f}^{N} \left\{ N_f - \left(n - N_f \right) \right\} l_{sp} \cos\left(\frac{p\pi n}{N} \right) dn \right] \tag{9}$$

which integrates to yield:

$$X_p = \frac{2 l_{sp} N}{p^2 \pi^2} \cos\left(\frac{p\pi N_f}{N} \right) - \frac{l_{sp} N}{p^2 \pi^2} \left[1 + \left(-1 \right)^p \right] \tag{10}$$

Thus, we have the following expressions for the first two modes:

$$X_1 = \frac{2 l_{sp} N}{\pi^2} \cos\left(\frac{\pi N_f}{N} \right) \tag{11}$$

$$X_2 = \frac{l_{sp} N}{2\pi^2} \left[\cos\left(\frac{2\pi N_f}{N} \right) - 1 \right] = -\frac{l_{sp} N}{\pi^2} \sin^2\left(\frac{\pi N_f}{N} \right) \tag{12}$$

In this study, we use the magnitudes of the modes, denoted by $\bar{X}_1$ and $\bar{X}_2$. The maximum values of the magnitudes of the first and second modes are reached when the chain is fully stretched and when there is a hairpin-like fold in the middle, respectively, and all the springs are stretched to their limit of νb_K, as discussed earlier. Let these maximum magnitudes be denoted as $\bar{X}_{1\max} = \frac{2\nu b_K N}{\pi^2}$ and $\bar{X}_{2\max} = \frac{\nu b_K N}{\pi^2}$. Then, we have the following:

$$\frac{\bar{X}_1}{\bar{X}_{1\max}} = \frac{l_{sp}}{\nu b_K} \cos\left(\frac{\pi N_f}{N} \right) \tag{13}$$

$$\frac{\bar{X}_2}{\bar{X}_{2\max}} = \frac{l_{sp}}{\nu b_K} \sin^2\left(\frac{\pi N_f}{N} \right) \tag{14}$$

The state of stretch of the springs is given by $\hat{r} = \frac{l_{sp}}{\nu b_K}$. Combining Eqs. (13) and (14), we get the following quadratic equation for $\hat{r}$:

$$\left(\frac{1}{\hat{r}}\right)^2\left(\frac{\bar{X}_1}{\bar{X}_{1\max}}\right)^2 + \left(\frac{1}{\hat{r}}\right)\left(\frac{\bar{X}_2}{\bar{X}_{2\max}}\right) = 1 \tag{15}$$

which gives the following solution for $\hat{r}$:

$$\hat{r} = \frac{1}{2}\left[\left(\frac{\bar{X}_2}{\bar{X}_{2\max}}\right) \pm \sqrt{\left(\frac{\bar{X}_2}{\bar{X}_{2\max}}\right)^2 + 4\left(\frac{\bar{X}_1}{\bar{X}_{1\max}}\right)^2}\right] \tag{16}$$

where we only consider the solution that is not negative. This solution can be rearranged as:

$$\hat{r} = \frac{1}{2}\left(\frac{\bar{X}_2}{\bar{X}_{2\max}}\right) + \sqrt{\left(\frac{1}{2}\frac{\bar{X}_2}{\bar{X}_{2\max}} + \frac{\bar{X}_1}{\bar{X}_{1\max}}\right)^2 - \left(\frac{\bar{X}_2}{\bar{X}_{2\max}}\right)\left(\frac{\bar{X}_1}{\bar{X}_{1\max}}\right)} \tag{17}$$

Thus, if $\left(\frac{\bar{X}_2}{\bar{X}_{2\max}}\right)\left(\frac{\bar{X}_1}{\bar{X}_{1\max}}\right) \ll \left(\frac{1}{2}\frac{\bar{X}_2}{\bar{X}_{2\max}} + \frac{\bar{X}_1}{\bar{X}_{1\max}}\right)^2$, we have a simple relationship:

$$\hat{r} = \frac{\bar{X}_2}{\bar{X}_{2\max}} + \frac{\bar{X}_1}{\bar{X}_{1\max}} \tag{18}$$

Eq. (18) is the sum of the two normalized normal mode magnitudes with equal weighting that was discussed earlier. In addition to being the simplest measure of deformation involving more than one normal mode, this result arises as an approximation to Eq. (17) under some conditions. Since both fractions are between 0 and 1, Eq. (18) will be a good approximation if one is much larger than the other. Typically, when the chain is highly stretched, the fraction $\frac{\bar{X}_1}{\bar{X}_{1\max}}$ is much larger than $\frac{\bar{X}_2}{\bar{X}_{2\max}}$, while the reverse is true when the chain is folded near its middle. Near equilibrium,

when the springs are not stretched, the fractions may be comparable. However, for such a case, the predicted spring constant will be close to the value at equilibrium, and insensitive to the approximation made. In fact, for all our simulations presented here, negligible difference is found in results when using Eq. (18) instead of Eq. (17).

Surprisingly, our results, presented later, show that that Eq. (18) is sufficient to model the dynamics quite accurately in all the flows considered here. The success of such a crude approach is surprising, and suggests that the largest inaccuracy of using only the magnitude of first mode to determine the spring constant is in its neglect of highly stretched chains with a single fold. Multiply-folded chains presumably either have effective spring constants that are not so high, or, even if the chain is highly stretched between the folds, the contribution of these configurations to the stress is evidently not so large. This conclusion is supported by an analysis showing that the contribution to the stress of locally stretched, but folded, polymer conformations, is proportional to the cube of the length of a fully stretched segment between folds [36]. Thus, the contributions to the stress of short folded regions, which would be captured by modes higher than the second, contribute little to the stress compared to the contribution of long folded regions, the longest of which constitutes around half the chain length.

Hence, to conclude, we have defined an effective fractional stretch at any given time:

$$\hat{r} = \frac{\bar{X}_1}{\left(\frac{2N\nu b_K}{\pi^2}\right)} + \frac{\bar{X}_2}{\left(\frac{N\nu b_K}{\pi^2}\right)} \tag{19}$$

We insert this into the Cohen-Padé approximation to estimate the value of f:

$$f = \frac{1}{3}\frac{3-\hat{r}^2}{1-\hat{r}^2} \tag{20}$$

The effective spring constant is then given as $k = Hf$, where, at equilibrium, H is the spring constant and $f = 1$. Thus, in this study, we consider the evolution of modes with an effective spring constant that varies with the values of the magnitudes of the first and second modes. Hence, our method reduces to an equation similar to the FENE-p approximation if: 1) we use only the longest mode to obtain the fractional stretch $\hat{r}$, and 2) we obtain the stress from only one mode. We obtain much better results by both using multiple modes to obtain the stress, thus including the faster relaxing processes, and by obtaining the spring constant from the two longest modes, not just the longest one. The latter innovation allows the spring constant to be influenced not only by the overall chain conformation, captured by the longest mode, but also to some extent by the internal conformation of the chain, captured by the second-longest mode, thus accounting for the influence of local stretch, not just global stretch, on the spring constant. As in other pre-averaging methods, we also average the spring constant over the ensemble of chains and moreover use the same spring constant for all modes, thus maintaining a much faster computation than in Brownian dynamics simulations, which requires simulating an entire ensemble of chains. It will soon become clear how greatly these fairly simple changes to the constitutive equation improve the resulting predictions. We note that here we include stress contributions from all modes allowed by the resolution of the model (i.e., the number of modes equals the number of springs.) However, it is possible to further speed the calculation by using only a limited number of slower modes, a possibility we briefly discuss at the end of this work.

Evolution of normal modes:

Here, all normal mode evolution equations are solved numerically with a small time step size to obtain the dynamic evolution of their magnitudes. For uniaxial extensional flow, equations (A8)

and (A10) in the Appendix are used to update the values of xx and yy components of all the normal modes. For shear flow, equations (A14) and (A20), in conjuction with (A21), in the Appendix, are used to solve for the temporal evolution of the yy, xx and xy components of all normal modes, respectively. For planar mixed flows, the relevant equations are (A27), (A28) and (A29) in the Appendix. These equations allow us to compute the values of mode variables at the next timestep, using the value of the representative spring constant at the current time step. At any given time, the spring constant is estimated using equations (19) and (20). Note that for a general flow field where an analytical solution may not be possible, we can integrate Eq. (8) to obtain the time evolution of the modes.

Thus, to summarize, the model presented in this article for any general flow field consists of the evolution of the normal modes (Eq. (8)), the relation $k_p = 2\pi^2 kp^2 / N$, and the expression for the nonlinearity f in the spring constant, $k = Hf$, given in Eqs. (19) and (20). Alternatively, the more accurate Eq. (17) can be used instead of Eq. (19), but we have found little difference between the two. In this study, we use an explicit Euler method for all time integrations of these equations.

Calculation of stress:

Using the magnitude of the normal modes, we calculate the components of the stress tensor using the following relation [35]:

$$\vec{\vec{\tau}} = n_C k_B T \left[\sum_{p=1}^{N} k_p \vec{c}_P - N\vec{\vec{\delta}} \right] \qquad (21)$$

where $k_p = 2\pi^2 kp^2/N$ and $k = Hf$, as defined earlier. $\vec{\vec{\delta}}$ is the isotropic tensor, n_C is the number of polymer chains per unit volume and $\vec{\vec{c}}_P = \left\langle \vec{X}_p \vec{X}_p \right\rangle$. Incorporating all these, Eq. (21) can be further written as:

$$\vec{\vec{\tau}} = n_C k_B T \left[\frac{6\pi^2 f}{N\nu b_K^2} \sum_{p=1}^{N} p^2 \vec{\vec{c}}_P - N\vec{\vec{\delta}} \right] \tag{22}$$

(The dimensionless stress values compared with BD simulations later in this article are normalized by n_C and $k_B T$.) We assess in Appendix B the consistency of the formula Eq. (21) for the stress tensor with the "virtual work" argument, which is typically used to demonstrate the existence of an elastic free energy function from which the stress tensor can be derived. We address the validity of the virtual work argument in Appendix B in the limits of modest spring stretch where the spring constant is not dependent on chain deformation, and provide an argument for consistency in the limit of strongly stretched springs, forming folded or fully stretched states of the molecule. A more complete assessment of thermodynamic consistency of the model awaits future work. However, the success of the model shown under a wide variety of conditions in the following is strong evidence that this limitation has little consequence on the model accuracy. In fact, as we discuss near the end of this paper and in Appendix B, the construction of a spring constant that is valid in the limit where the polymer is locally nearly fully stretched, and therefore highly dissipative under flow, is likely a key to the success of the model in fast nonlinear flows. We show below that the high rate of dissipation predicted by the model when the chain is highly stretched, is consistent with the behavior of the Brownian dynamics simulations, and likely makes the need for an elastic free energy at high chain stretch of relatively minor importance.

Results and discussion:

As discussed earlier, we will show detailed comparisons of our "FENE-mode" predictions with BD simulations for a variety of flow fields, starting with uniaxial extension. For all cases, we will consider a wide range of values of Weissenberg number (Wi) and two different chain contour lengths (in terms of the number of Kuhn steps). The Weissenberg number is the product of the strain rate and the longest stress relaxation time, as defined in previous work [24]. For all figures, most of the predictions from the BD simulations are averaged over an ensemble of several hundred chains. The exact numbers of chains used to compute the average behavior are given in the figure captions. Most of the BD simulations are performed using the coarse-grained bead-spring representation, whose details are provided elsewhere [24]. For a few BD simulations, we have used a stiff Fraenkel spring, which mimics a single Kuhn step (or "rod") that is nearly inextensible [24-25]. These are denoted by "BR", denoting "bead-rod". The cases denoted as "CG" have used the Cohen-Padé approximation for the spring law.

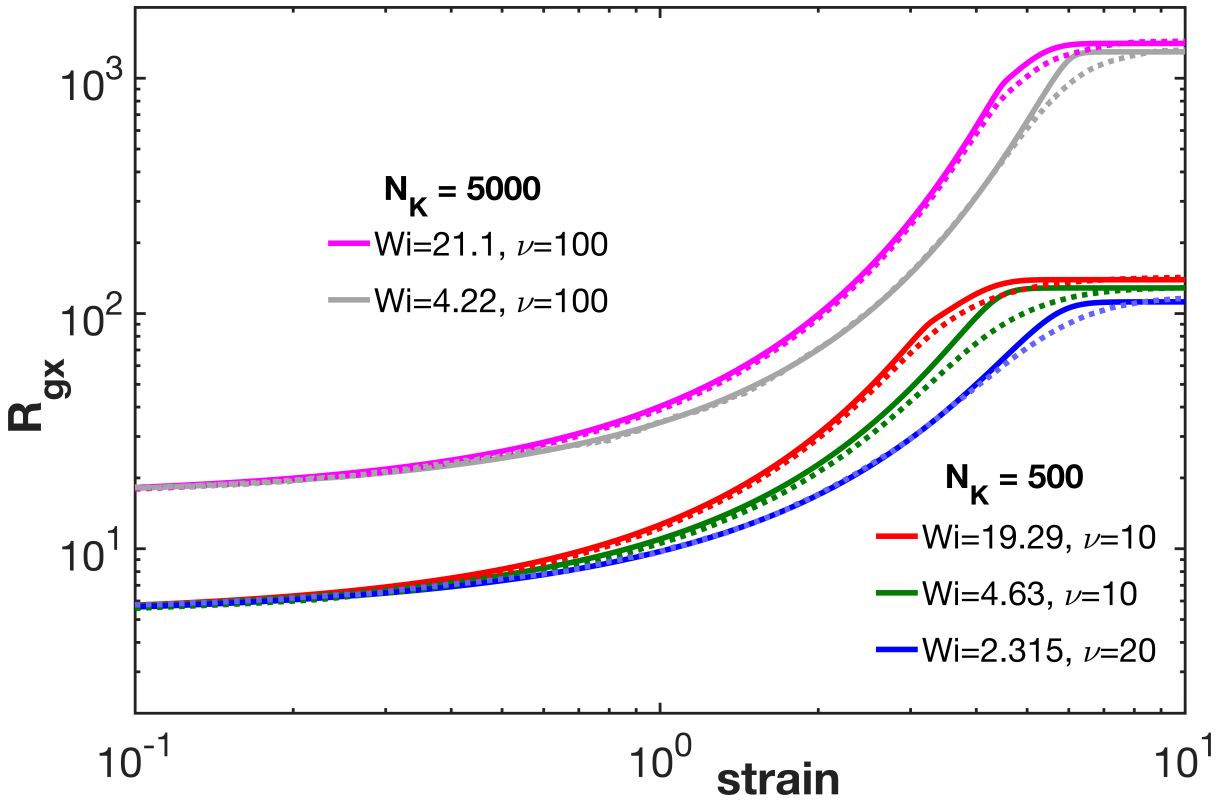

Figure 2: Comparison of the predictions of BD simulations (dotted lines) and FENE-mode (solid lines) for the strain dependence of the chain radius of gyration in the flow direction R_{gx} in startup of uniaxial extensional flow for two different polymer chains – consisting of 500 and 5000 Kuhn steps (denoted by N_K in the legends). For each run, the legend shows the value of Wi. The terms "BD" and "FENE-mode" indicate results from BD simulations and predictions from the FENE-mode models, respectively. For BD simulations, a bead-spring model, with the Cohen-Padé approximation serving as the spring law, is used. The number of Kuhn steps encompassed by a single spring is given by ν. The number of chains over which the BD simulations are averaged are: 400, 1200 and 1200 for Wi = 2.315, 4.63 and 19.29, respectively, for N_K = 500; 50 and 100 for Wi = 4.22 and 21.1., respectively, for N_K = 5000.

Figures 2-5 highlight the success of the FENE-mode model in predicting both overall chain conformation and stress in uniaxial extensional flow. In Fig. 2, we compare results of the FENE-mode model with "exact" BD simulation results for the temporal evolution of the chain radius of gyration in the flow direction R_{gx}, defined precisely in earlier studies [24]. The results are plotted against Hencky strain, which is the product of the strain rate and time. Clearly, the FENE-mode predictions (solid lines) are in good agreement with those obtained from the BD simulations (dotted lines), across a range of *Wi* and chain length. Figure 3 compares the transient extensional stress in startup, again showing the success of the FENE-mode model. (Note that, owing to computational limitations, for BD simulations, the results are somewhat noisy at small strains.) Across all *Wi* considered, for two very different chain lengths, the predictions of the FENE-mode model, including the final steady state values, are in excellent agreement with BD simulations. Figures 4 and 5 show the steady-state values of the chain stretch (i.e. R_{gx}) and the thickness in the transverse direction (i.e. R_{gy}), respectively. Again, we observe an excellent match between the values obtained from the FENE-mode and BD simulations. Figures 2-5 show agreement between FENE-mode and BD simulations that is usually within 20% or so, with larger deviations generally confined to small regions of time or strain rate, such as the region of steeply increasing R_{gx} in Figure 4. Similar agreement is shown in the other figures displayed in what follows.

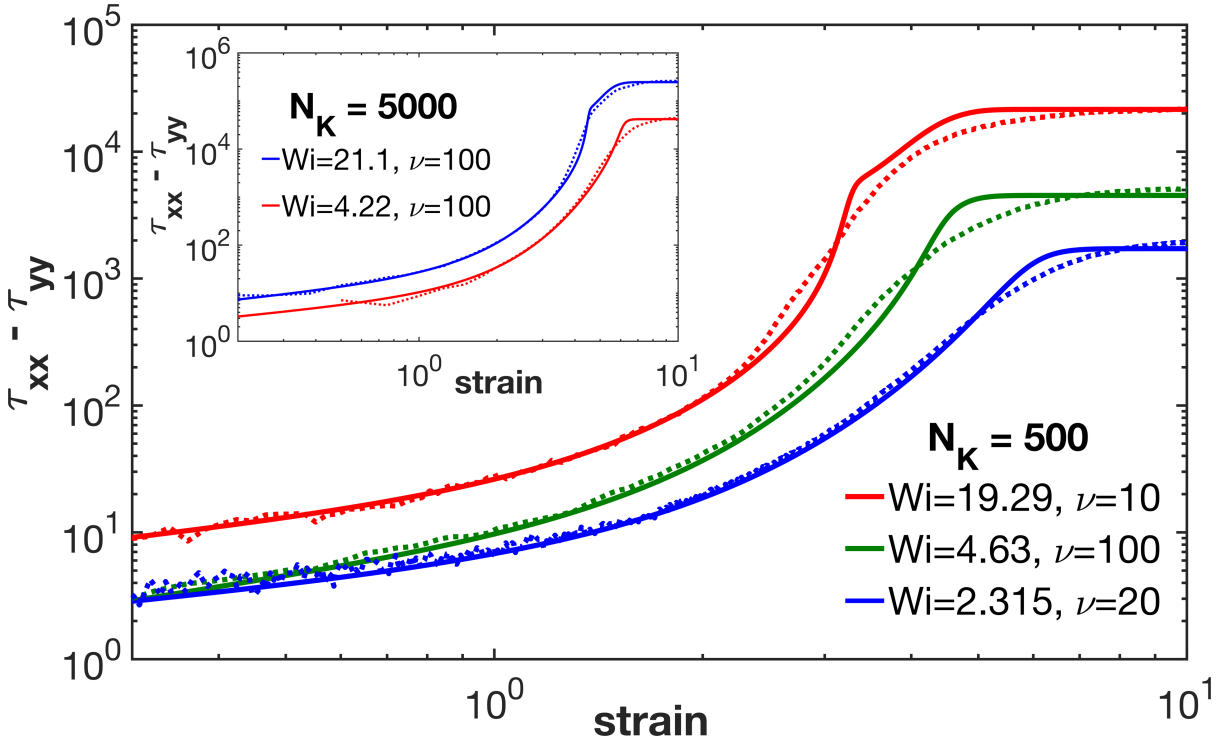

Figure 3: The same as Figure 2, except for the extensional stress given by the normal stress in the flow direction minus that perpendicular to it. Here, x represents the extensional flow direction. The inset shows results for a longer chain of 5000 Kuhn steps.

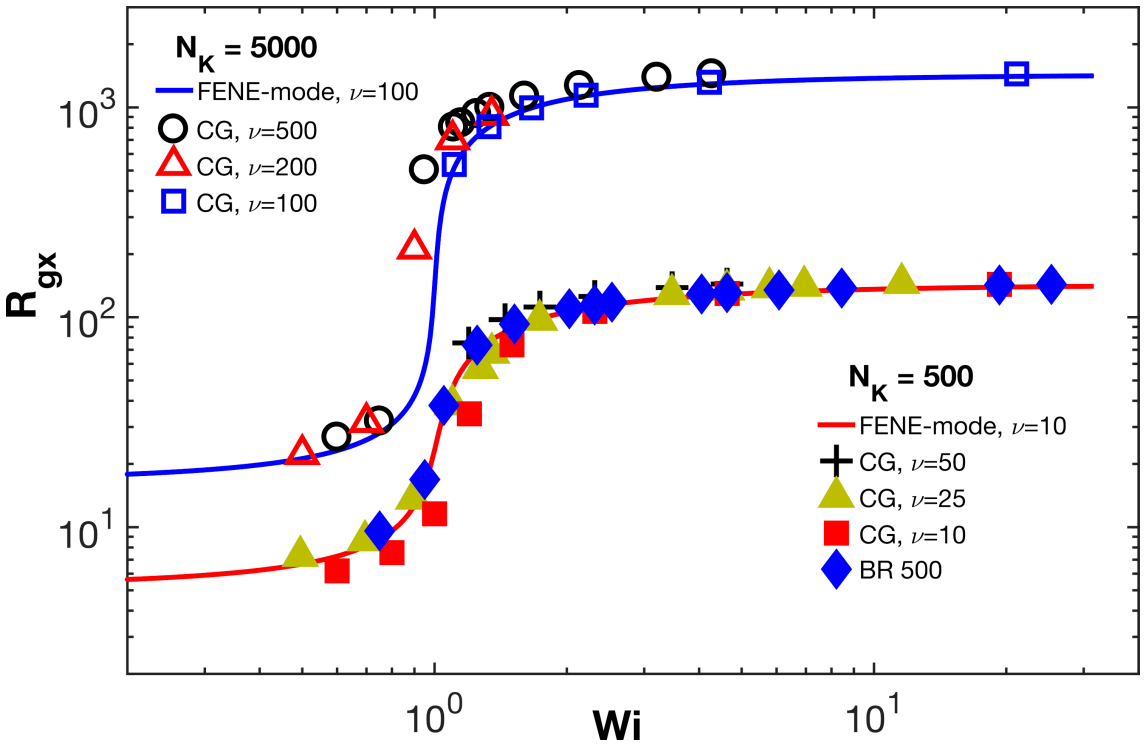

Figure 4: Predictions of BD simulations and FENE-mode model for the final steady state values of R_{gx} in uniaxial extensional flow for chain lengths of 500 and 5000 Kuhn steps, with ν denoting the number of Kuhn steps per spring. Here, the term "CG" denotes a bead-spring model, with the Cohen-Padé approximation used as the spring law. The term "BR" indicates that stiff Fraenkel springs are used, each of which represents a single Kuhn step, for BD simulations (details given in earlier study [24]). Note that the legends are divided into two groups for the two different chain lengths considered.

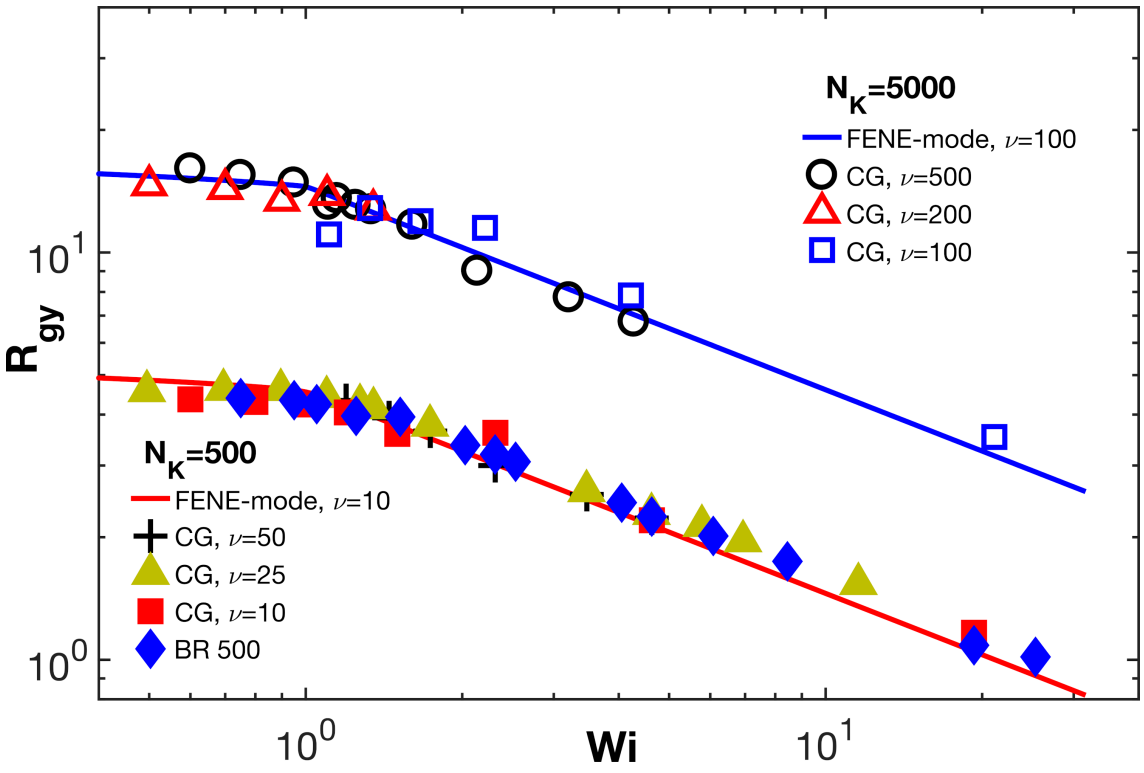

Figure 5: Predictions of BD simulations and FENE-mode for the steady-state values of the chain "thickness" R_{gy} in uniaxial extensional flow. The legends are the same as in Figure 4 (description is provided in the caption of Figure 4).

Next, we test the FENE-mode for the polymer dynamics in steady shear flow, which has been thoroughly investigated by BD simulations in earlier articles [8, 24-26]. Figure 6 shows the strain dependence of R_{gx} at different values of *Wi* for two different chain lengths. Since the steady state in shear flow is an ensemble average over chains undergoing incessant tumbling events, a large number of chains are needed to obtain an accurate average, but even so, there is significant noise in the BD results. However, within the limits of the noise, the FENE-mode predictions are in excellent agreement with all the BD simulations considered for this study. Similar performance of FENE-mode is observed for the two important rheological measurements – the first normal stress

difference and the shear stress, presented in Figs. 7 and 8, respectively. At high values of Wi, an overshoot is visible in our data from BD simulations, consistent with observations reported in earlier studies [7]. Remarkably, the predictions of the FENE-mode model are in outstanding agreement with all the trends obtained from the BD simulations, including the magnitude and position of the overshoot at higher *Wi* and the final steady state values. Further, the predictions of the radius of gyration in both the flow direction R_{gx} (Fig. 9) and flow gradient direction R_{gy} (Fig. 10) are in excellent agreement with BD results across all regimes reported earlier [24]. The FENE-mode slightly under-predicts the values of R_{gy} but is consistent with the scaling law obtained for the chain thickness in shear flow (marked in Fig. 10) for bead-spring chains.

In addition to these common flow fields, as a further check, we performed BD simulations for planar mixed flows, where $\hat{\kappa}$ is defined as [20]:

$$\hat{\kappa} = \dot{\gamma}\begin{bmatrix} 0 & 1 & 0 \\ \alpha_{\text{flow}} & 0 & 0 \\ 0 & 0 & 0 \end{bmatrix} \tag{25}$$

where the flow type is controlled by the parameter α_{flow}. The values α_{flow} = 1, 0 and -1 denote planar extension, simple shear, and pure rotational flow, respectively. For BD simulations with mixed flows, we selected values of 0.5 and -0.5 for α_{flow}. The first of these denotes a flow half-way between extension and shear $\left(\alpha_{\text{flow}} = 0.5\right)$ (and the other a flow half-way between shear and pure rotation $\left(\alpha_{\text{flow}} = -0.5\right)$.

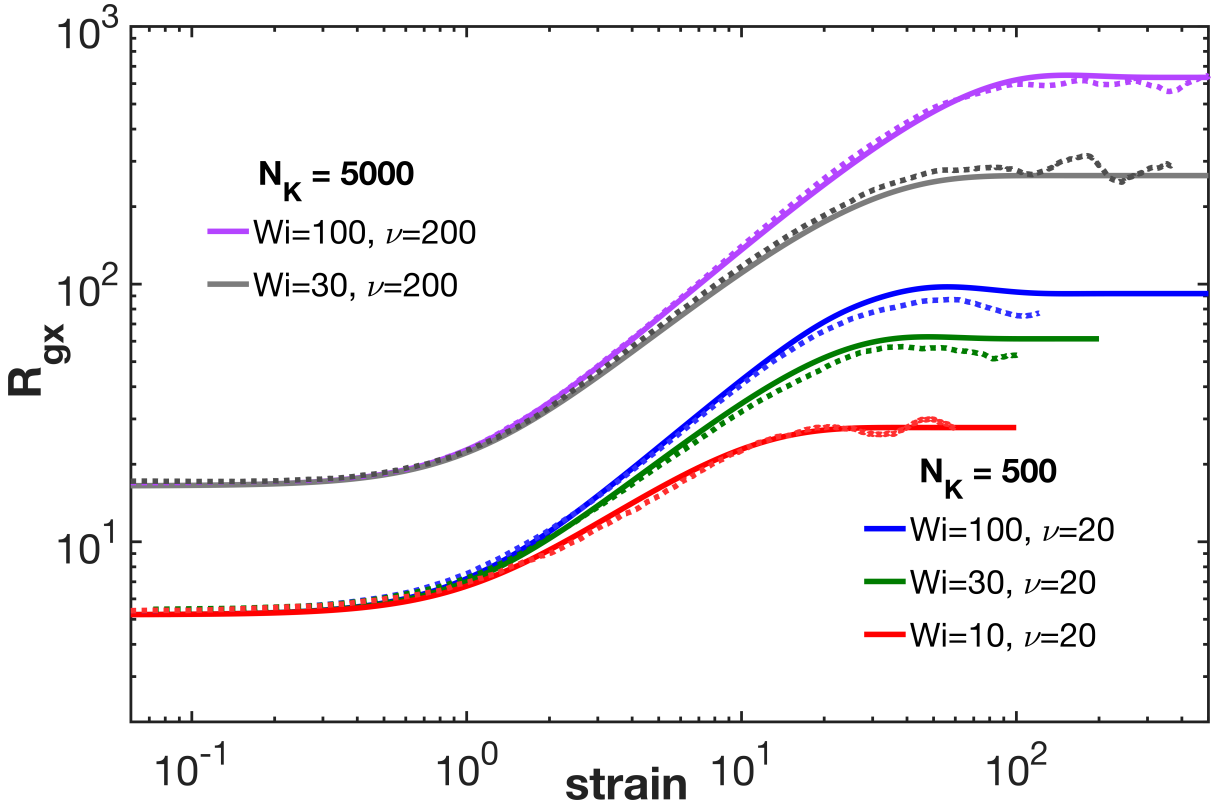

Figure 6: Predictions of BD simulations with ν Kuhn steps per spring and FENE-mode model for the strain dependence of R_{gx} in startup of shear flow. Other details are the same as in Figure 2. The number of chains averaged over in the BD simulations are: 150, 200 and 100 for Wi = 10, 30 and 100, respectively, for N_K = 500; 150 and 100 for Wi = 30 and 100, respectively, for N_K = 5000.

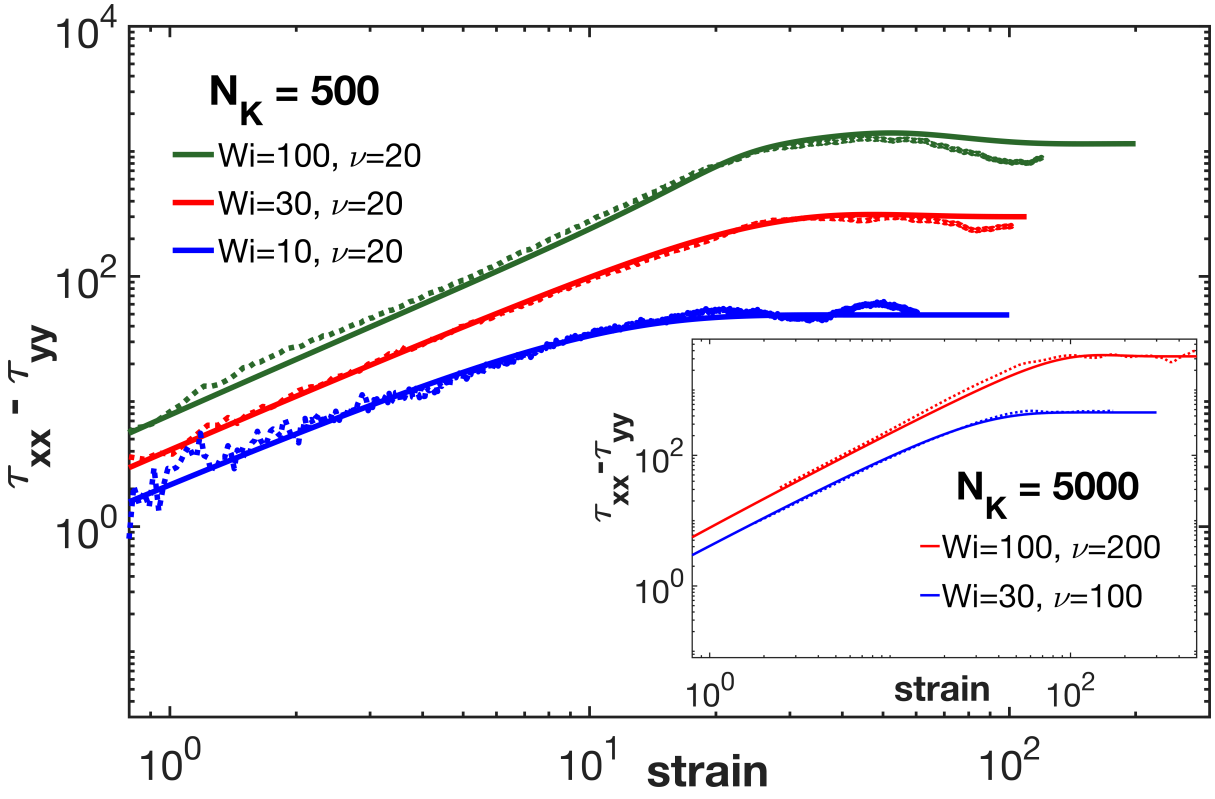

Figure 7: The same as Figure 6, but for the first normal stress difference. Here, x and y represent the flow and gradient directions, respectively. The inset shows results for a longer chain of 5000 Kuhn steps. In the inset, the symbols and solid lines indicate results from BD simulations and FENE-mode, respectively.

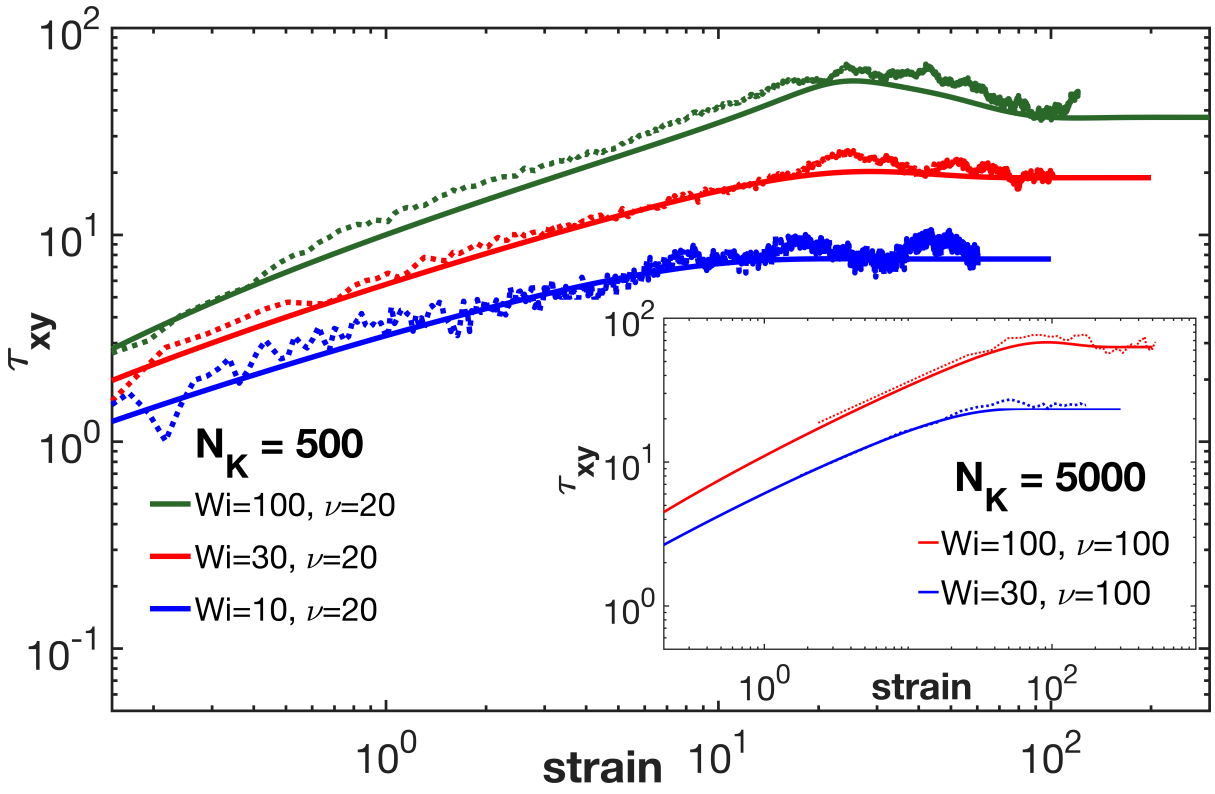

Figure 8: The same as Figure 6, except for the shear stress. The inset shows results for a longer chain of 5000 Kuhn steps. In the inset, the symbols and solid lines indicate results from BD simulations and FENE-mode, respectively.

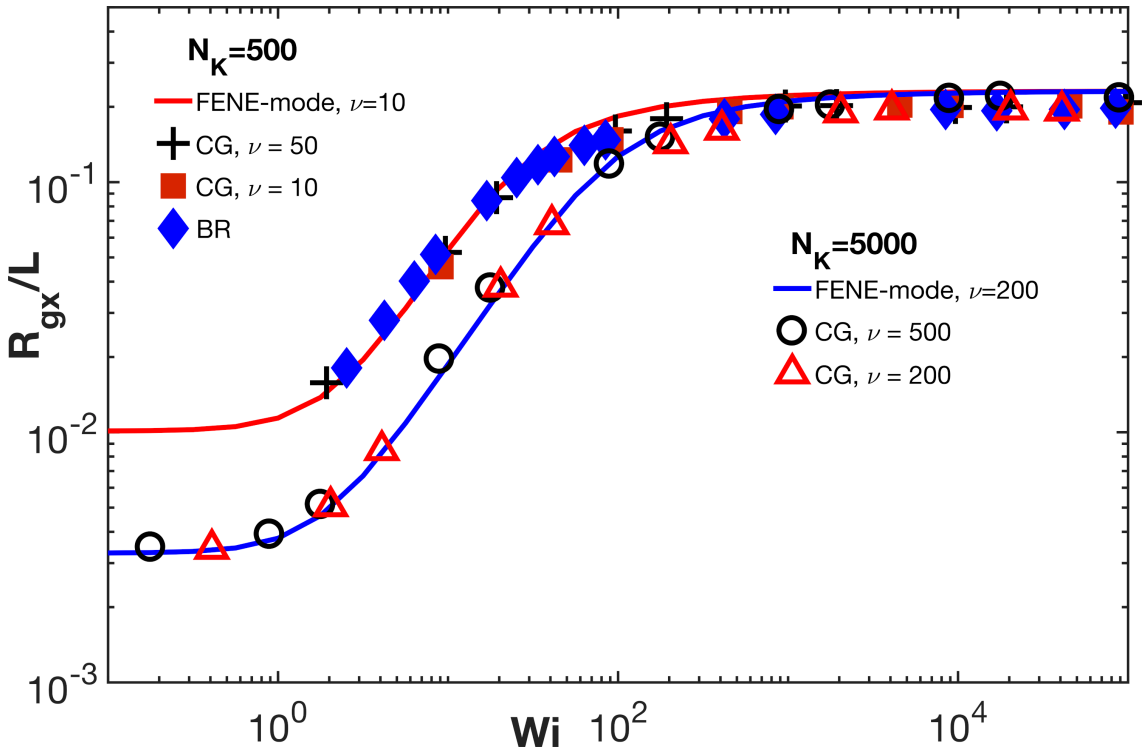

Figure 9: Comparison of the predictions of coarse-grained (CG) and fine-grained bead-rod (BR) BD simulations and FENE-mode for the steady state values of R_{gx} in steady shear. Other details are the same as in Figure 5.

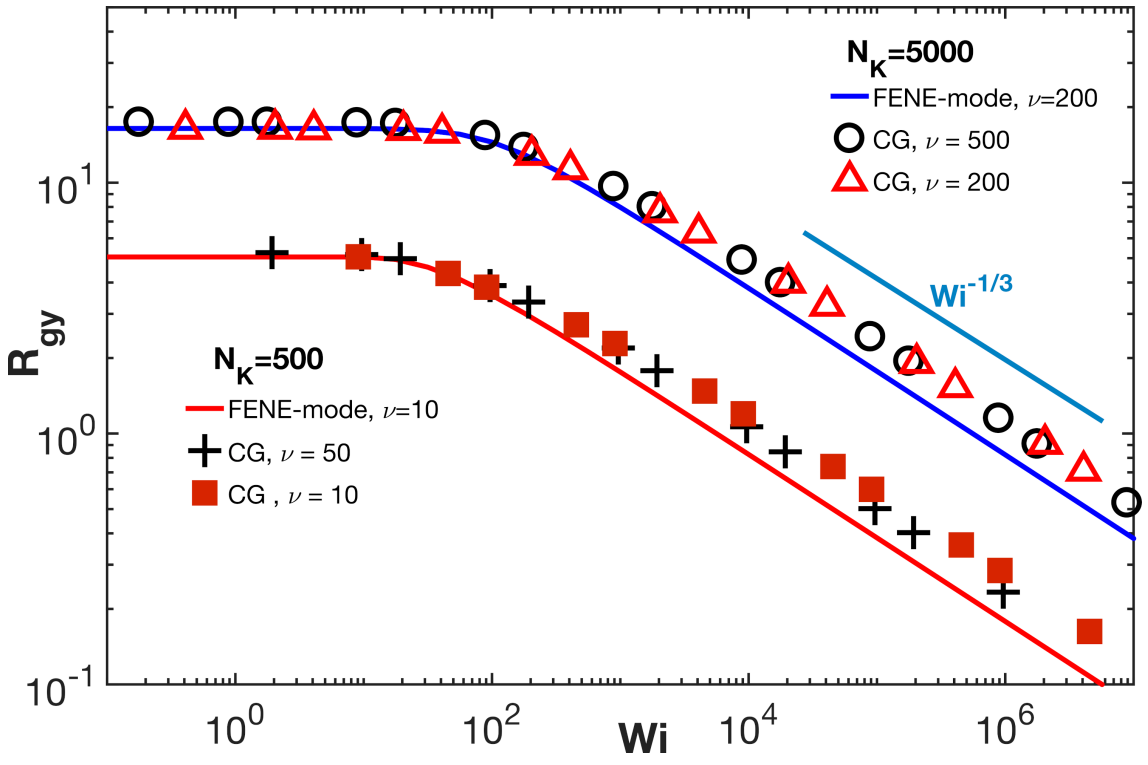

Figure 10: The same as in Figure 9, except for the chain thickness R_{gy}. The scaling law of $Wi^{-1/3}$ for BD simulations using the bead-spring chains has been reported earlier in literature [24-25].

In Figures 11-13, we present the temporal evolution of the chain overall radius of gyration R_g, the first normal stress difference $\tau_{xx} - \tau_{yy}$, and the shear stress τ_{xy}, for various *Wi*, for two different chain lengths, for $\alpha_{\text{flow}} = 0.5$. The trends are qualitatively similar to those obtained for extensional flow. As in the earlier cases with extension and shear, the agreement between the FENE-mode predictions and BD simulations is exceptional for all cases considered. We also performed BD simulations for a flow field that lies between shear and pure rotation $\left(\alpha_{\text{flow}} = -0.5\right)$. For this, we only show the transient behavior of the chain size (R_g) in Fig. 14. Owing to the dominance of rotation in this flow, the chain shows oscillations in the ensemble-averaged R_g with time, with little stretch (i.e., the maximum value of R_g is within 8% of the equilibrium value). It is noteworthy

that, even for this case, the FENE-mode predictions for the position and amplitude of the peaks are in extremely good agreement with those obtained from BD simulations. Overall, these observations further bolster our belief in the accuracy of the FENE-mode model for such simulations.

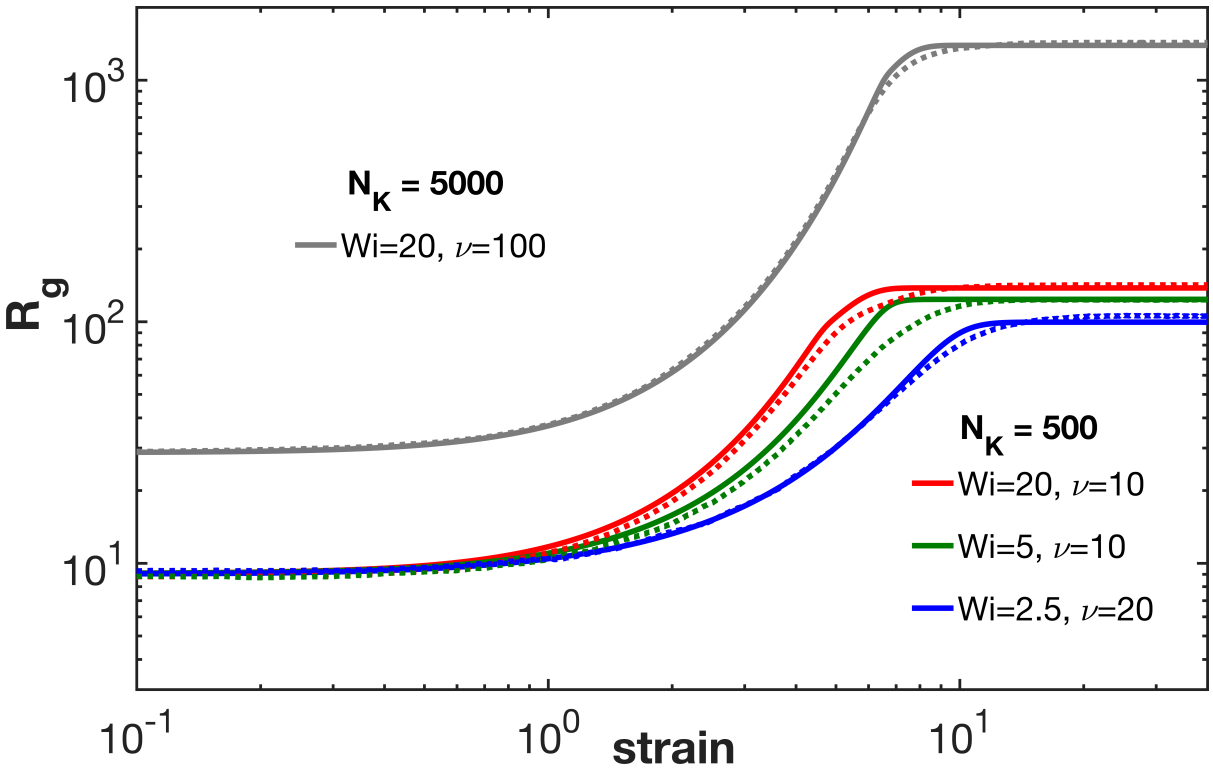

Figure 11: Predictions of BD simulations and FENE-mode for the strain dependence of the overall size of the chain R_g in startup of a planar mixed flow intermediate between extension and shear $\left(\alpha_{\text{flow}} = 0.5\right)$. Other details are the same as in Figure 2. Here, the number of chains over which the BD simulations are averaged are: 200, 100 and 100 for Wi = 2.5, 5 and 20, respectively, for N_K = 500 and 160 for N_K = 5000 (Wi = 20).

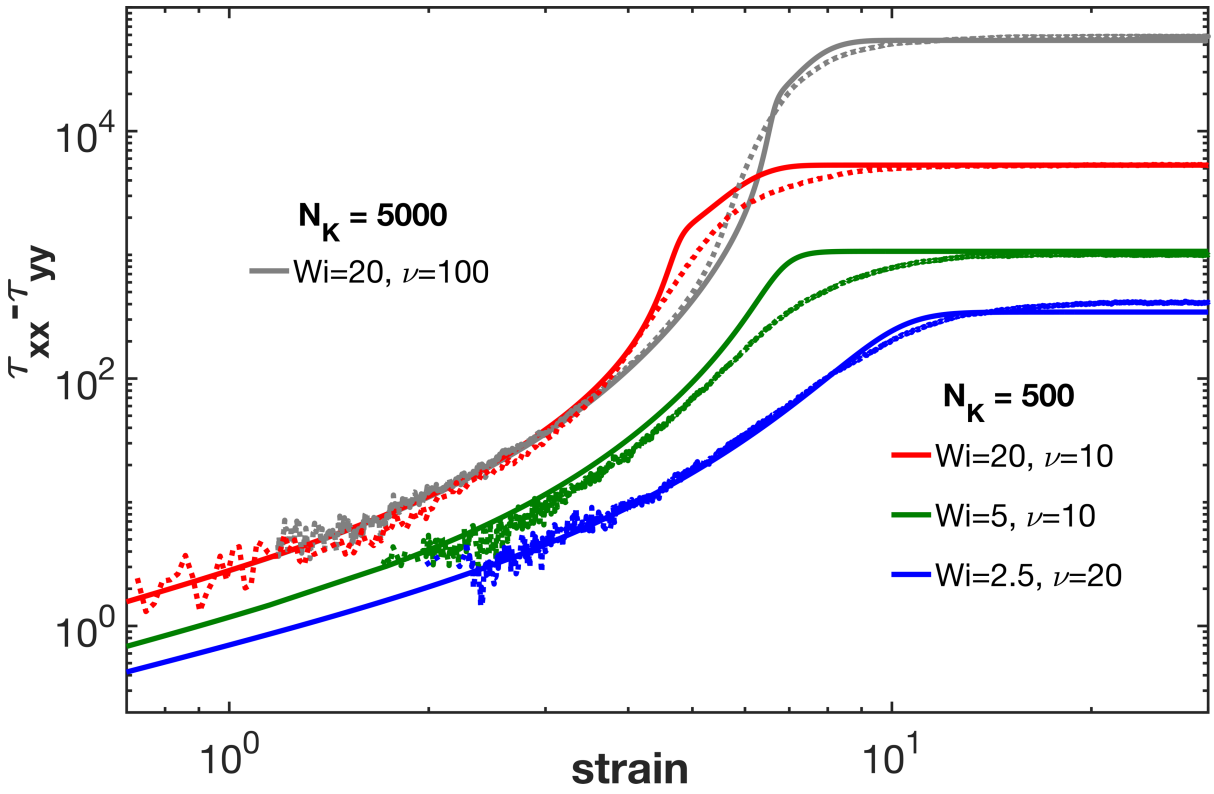

Figure 12: The same as in Figure 11 except for the first normal stress difference.

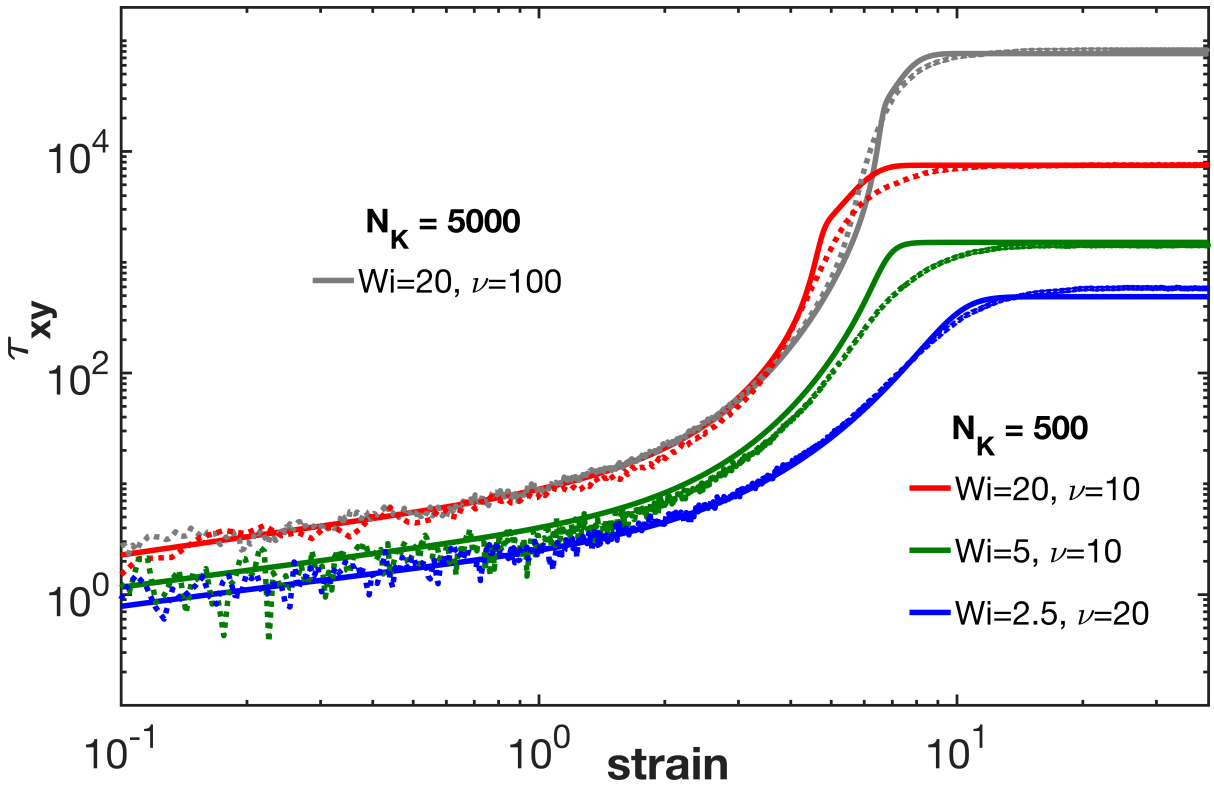

Figure 13: The same as in Figure 11, except for the shear stress.

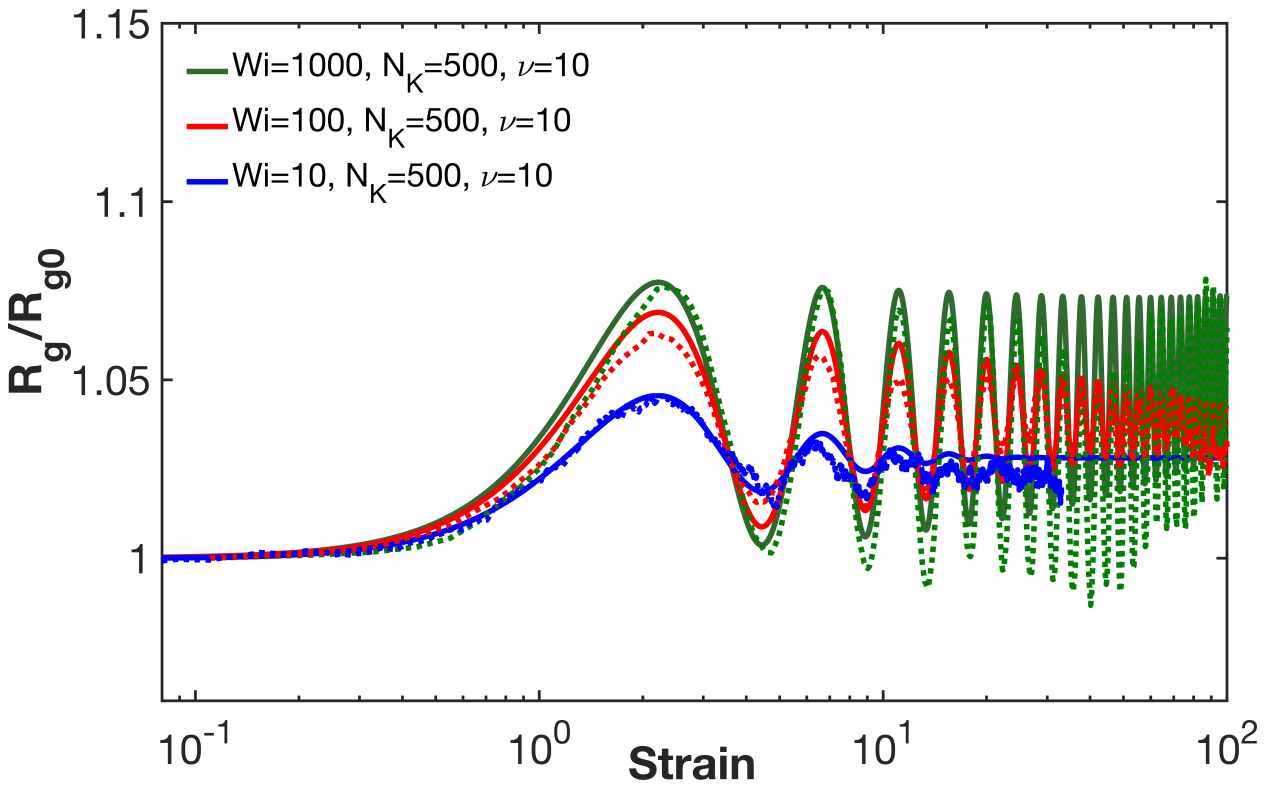

Figure 14: The same as in Figure 11, except for a planar mixed flow between shear and pure rotation $\left(\alpha_{\text{flow}} = -0.5\right)$. Here, R_g is normalized with respect to R_{g0}, its value at equilibrium. The number of chains over which BD simulations are averaged are 2400, 1000 and 100 for Wi = 10, 100 and 1000, respectively.

Next, in Figures 15 and 16, we compare some rheological predictions obtained from the FENE-mode model with those for FENE-P models. The FENE-P model is based on a dumbbell, and so is expected to perform more poorly than the FENE-mode model, which contains information on all the modes (even though the representative spring constant is estimated using only two modes). Note that the FENE-P model is incorporated into commercially available computational fluid dynamics (CFD) packages like ANSYS POLYFLOW and COMSOL, which can be used to study any transport problem that involves polymer solutions. The results for the first normal stress

difference for uniaxial extension in Figure 15 shows that the FENE-P model captures the trends satisfactorily, but the FENE-mode model provides superior predictions at all strains. The difference between the two models becomes even clearer for the shear stress in shear flow, shown in Fig. 16, where the FENE-P shows the trends qualitatively, but the overall agreement with the results of simulations is poor. For the same flow, the FENE-mode shows excellent agreement with simulations, including the position and magnitude of the overshoot for higher values of *Wi*.

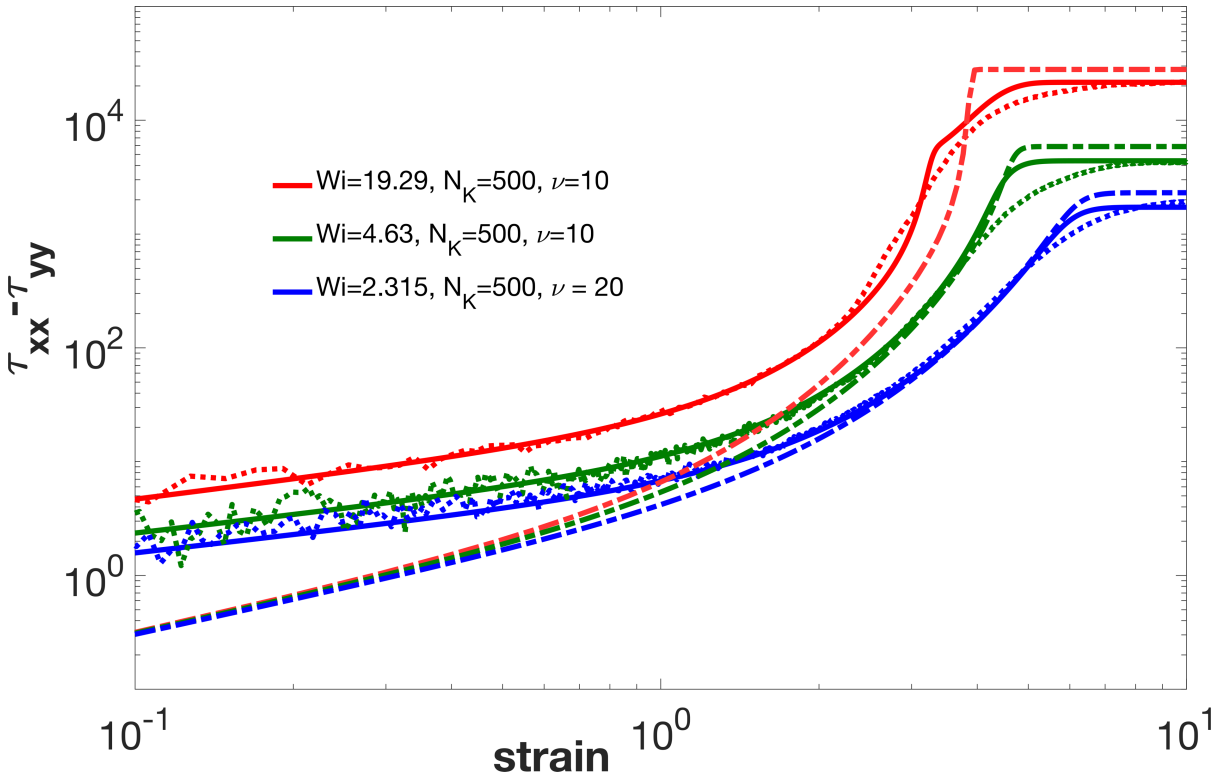

Figure 15: Predictions of BD simulations (dotted lines), FENE-P (dash-dotted lines) and FENE-mode (solid lines) models for the strain dependence of the extensional stress in startup of uniaxial extensional flow for polymer chains with 500 Kuhn steps. Other details are as in Figure 3.

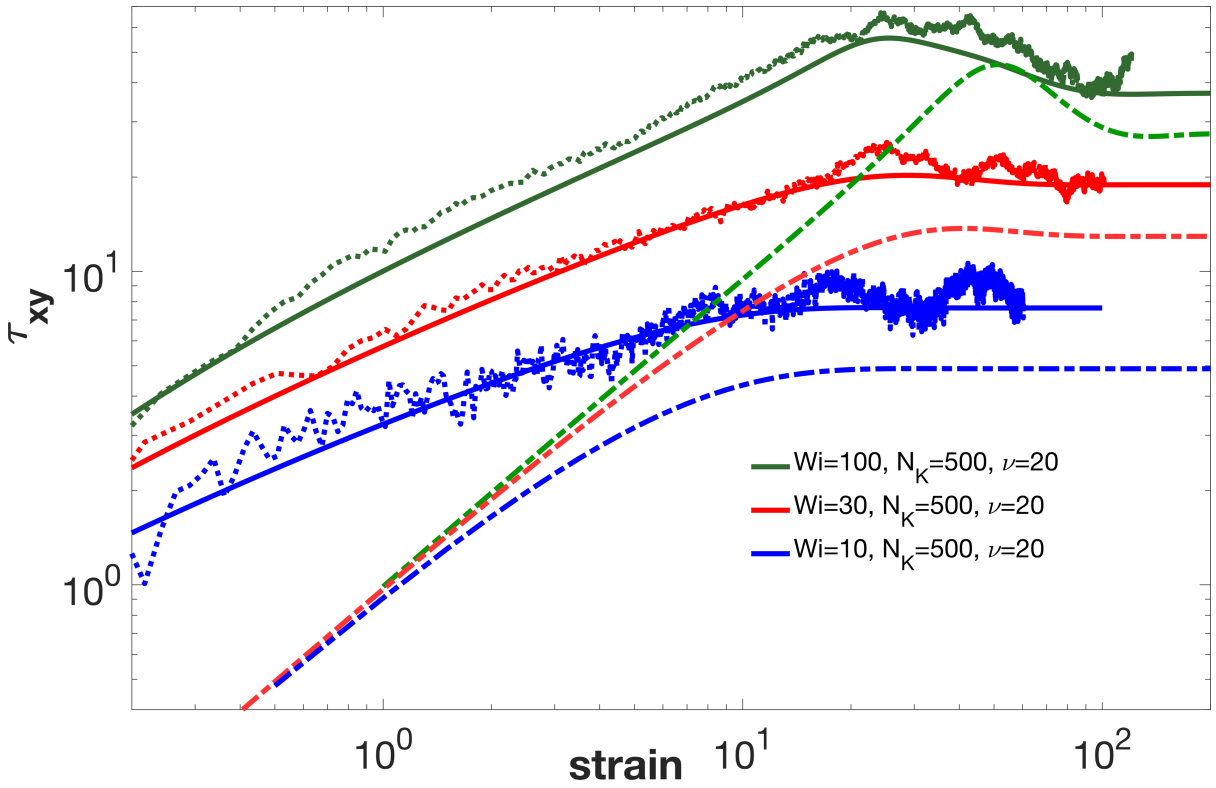

Figure 16: The same as Figure 15, except for shear stress in startup of shear flow. Note that the results from the BD simulations are shown by dotted lines, FENE-P by dash-dotted lines and FENE-mode by solid lines.

To explore this further, we compare the FENE-mode predictions, for varying number of modes, with BD simulations and FENE-P in Figures 17 and 18. For the normal stress difference at a fixed uniaxial extension flow rate (Fig. 17), the FENE-mode model shows a systematically increasing deviation from BD simulation results at low strains, as the number of modes is lowered. For a single mode FENE-mode model, the results are almost the same as for the FENE-P model. At higher strains, all the models agree well with one another. The comparison for the shear stress at a fixed shear rate is shown in Fig. 18. As in Fig. 17, systematic deviations increase at low strains as the number of modes are decreased in the FENE-mode model. The single-mode FENE-mode

prediction is almost the same as that of the FENE-P model, as is the case in uniaxial extension. However, significantly, at high strains, the FENE-mode model with just two modes agrees reasonably well with the BD simulations, whereas the FENE-P model shows significant deviations. Thus, the FENE-mode with just two modes provides much better predictions than FENE-P model, especially for shear flows.

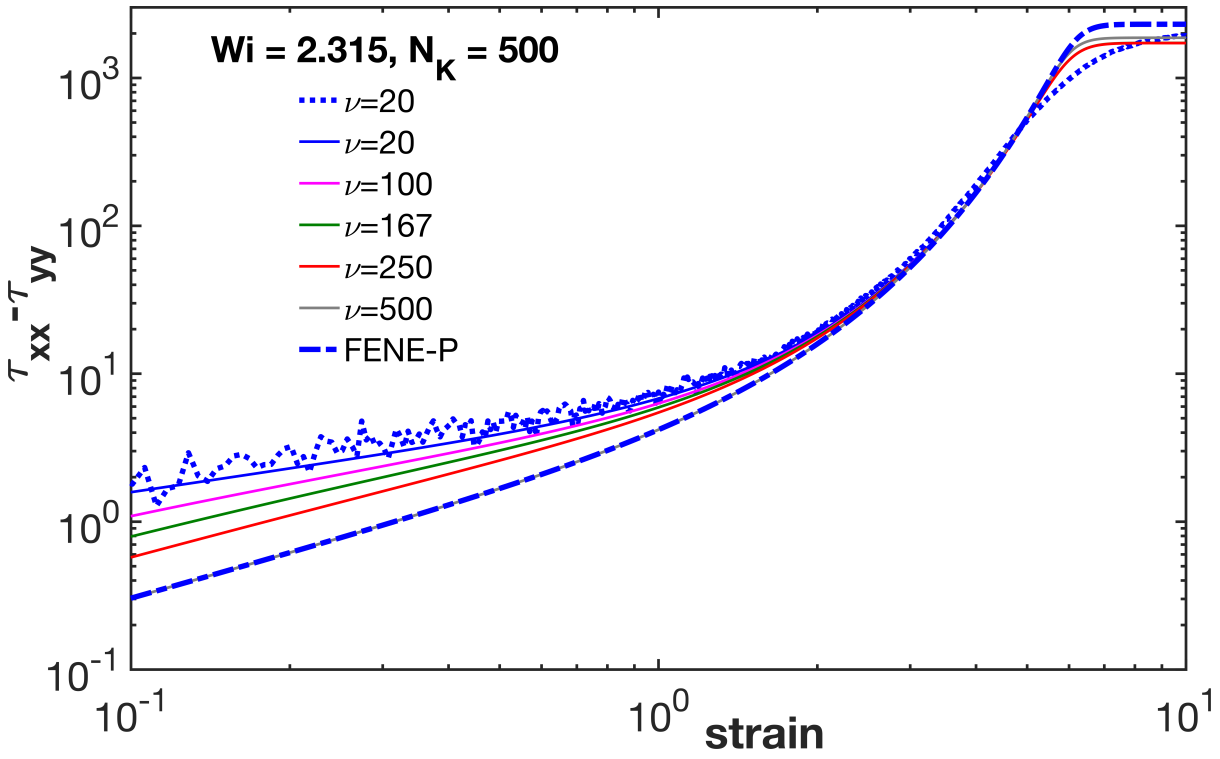

Figure 17: Predictions of the strain dependence of the extensional stress in startup of uniaxial extensional flow (for Wi = 2.315) for polymer chains with 500 Kuhn steps from the FENE-mode model, for varying number of modes (solid lines). BD simulations (dotted line) are performed for $\nu = 20$ Kuhn steps per spring. The FENE-P results are shown by the dash-dotted line.

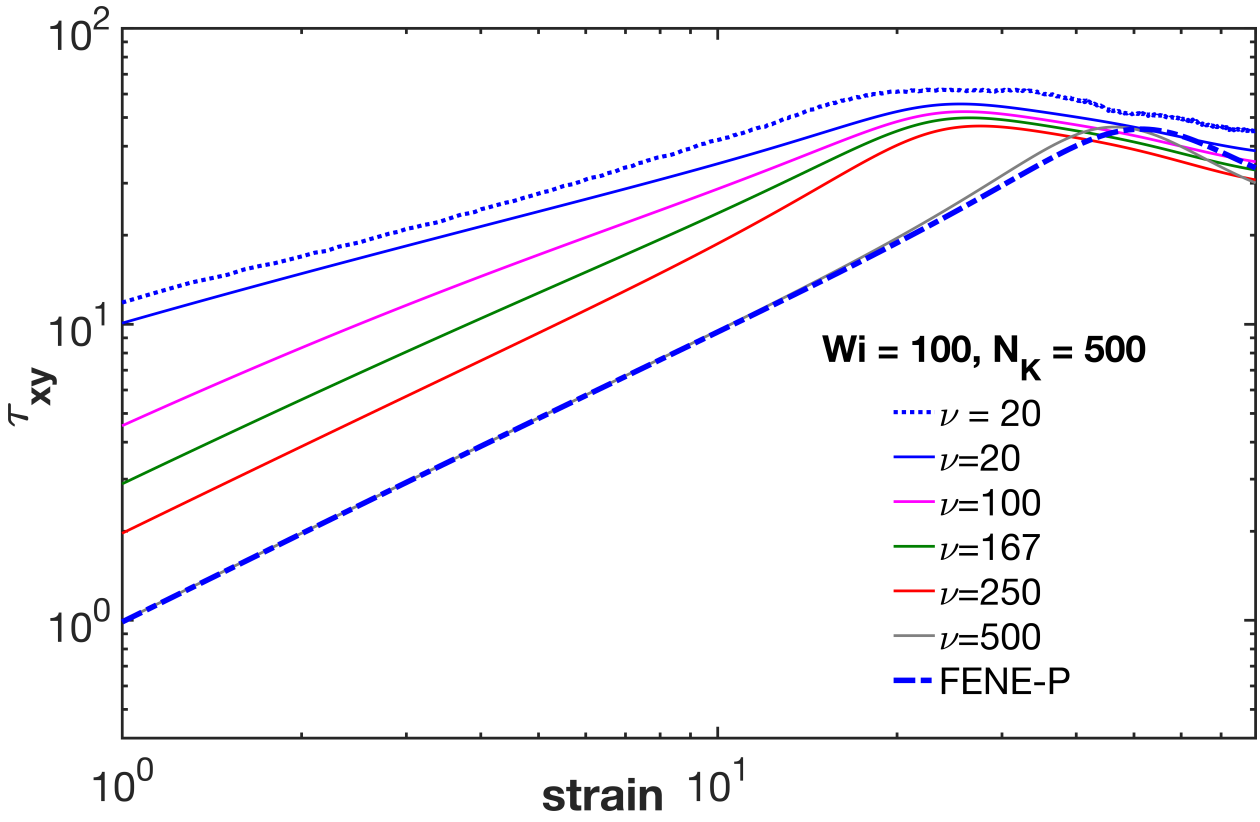

Figure 18: The same as Figure 17, except for shear stress in startup of shear flow (Wi = 100). Note that the results from the BD simulations are shown by dotted line, FENE-P by dash-dotted lines and FENE-mode (for varying ν) by solid lines.

Next, we show a few comparisons with the FENE-PM [38] and the multimode FENE-P [39] models to highlight the superiority of the FENE-mode model. The FENE-PM is a pre-averaged model that solves for the N normal modes at every timestep, similar to the FENE-mode, which therefore will have similar computational cost. However, the multimode FENE-P has to solve for N^2 equations at every timestep, and so for large numbers of modes will be much more expensive than the FENE-mode. Figure 19 show the results for the "stress-conformation" hysteresis loop, of stress cross-plotted against conformation, as defined in the caption of Figure 19, for extensional flow that is stopped after 5 strain units, for two different values of Wi. Clearly, magnitude of the hysteresis predicted by the FENE-mode predictions is in much better agreement with the BD

simulations than is that of the multimode FENE-P and the FENE-PM models. The forward and backward paths for the FENE-PM model are nearly identical, resulting in an almost non-existent hysteresis loop, similar to the observations in an earlier study [40]. While the multi-mode FENE-P model predicts some hysteresis, it predicts much less than in the BD simulations or the FENE-mode model, and is much more expensive computationally than the FENE-mode model.

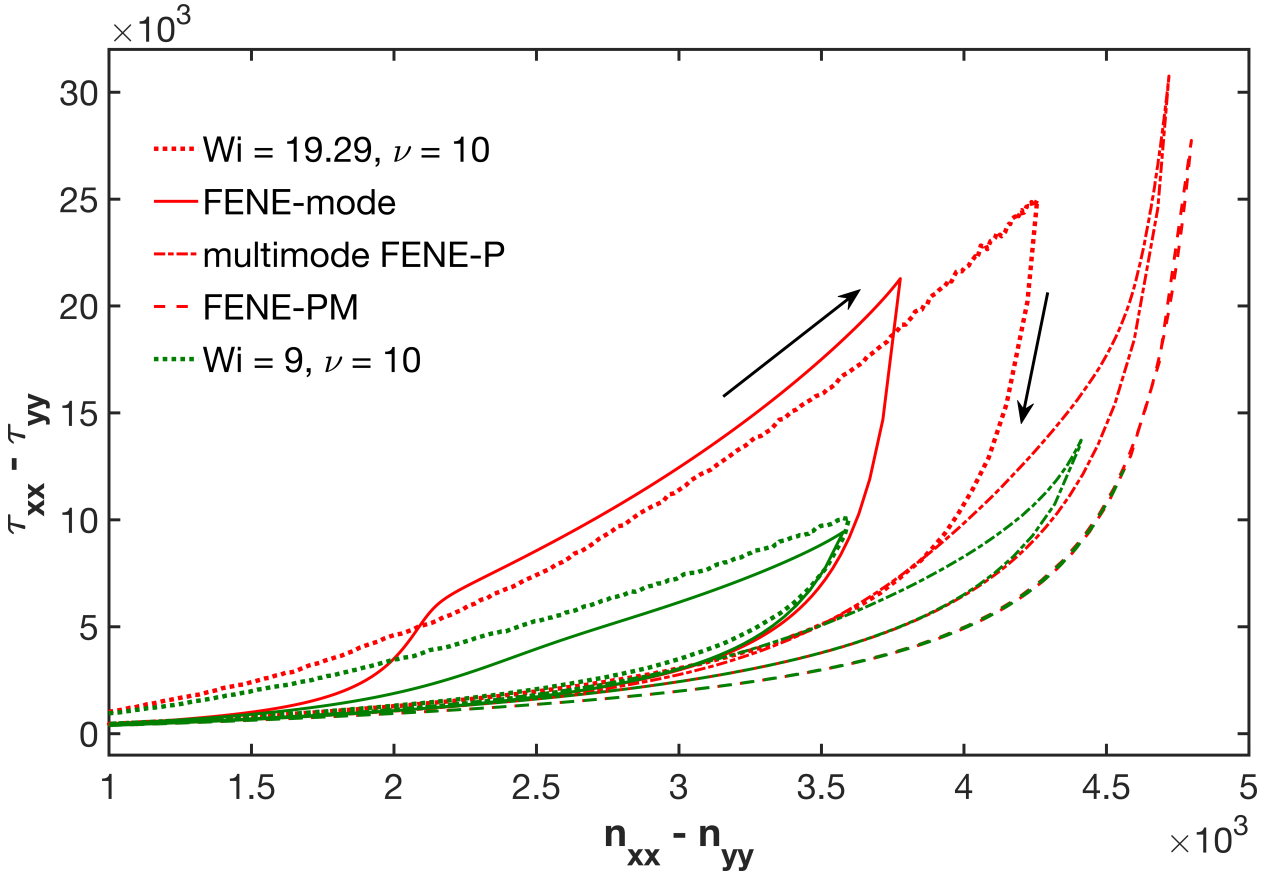

Figure 19: Stress-conformation hysteresis loops for uniaxial extensional flows of Wi = 9 and 19.29, when the flow was stopped after 5 strains. The results from the BD simulations for a chain of N_K = 500 and $\nu = 10$ are shown by dotted lines. The predictions of the FENE-mode, multimode FENE-P and FENE-PM models are shown by solid, dash-dot and dashed lines, respectively. The results for Wi = 9 and 19.29 are shown in green and red colours, respectively. Note that "conformation" here is taken to be the difference between the xx and yy components of the tensor

$\vec{n} = \sum_{i=1}^{N} \left\langle \vec{Q}_i \vec{Q}_i \right\rangle$, which is closely related to the birefringence measured experimentally. In the FENE-mode model, $\vec{n}$ can be calculated as $\vec{n} = \sum_{p=1}^{N} \frac{2\pi^2 p^2}{N} \left\langle \vec{X}_p \vec{X}_p \right\rangle$.

Here, note that the multi-mode FENE-P, while approximate relative to BD simulations, allows each spring its own spring constant, while FENE-PM uses a single spring constant for the whole chain, obtained from all the modes. The FENE-mode model is similar to FENE-PM in that it uses the same spring constant for each mode and uses only one equation per mode, but the FENE-mode model only uses the longest two modes to extract the spring constant. Thus, it might seem surprisingly, that, despite what appears to be a highly approximate treatment, the FENE-mode model provides much better agreement with the BD simulations for the stress-conformation hysteresis than does the FENE-PM model and even the multi-mode FENE-P model. This is likely due to a better accounting in the FENE-mode model of the underlying physics for the transient folded state, albeit the simplest possible one with a single fold in a one-dimensional chain, as revealed in earlier studies [24-25].

To explain in more detail, as noted in the article by Wedgewood et al. [38], for the FENE-P force law, we have

$$\vec{F}_j = HZ_j \vec{Q}_j \tag{26}$$

where the FENE factor for spring *j*, Z_j, is given by

$$Z_j = \frac{1}{1 - \left\langle \left(\frac{Q_j}{Q_0} \right)^2 \right\rangle} \tag{27}$$

where $Q_0 = \nu b_K$. For the FENE-PM chain, the index *j* is not needed, and Z is defined as

$$Z = \left[1 - \left(\frac{1}{Q_0^2 (N-1)} \right) \sum_{j=1}^{N-1} \left\langle Q_j^2 \right\rangle \right]^{-1} \tag{28}$$

Here, Z is related to the sum of mean squares of the magnitudes of all spring lengths, $\sum_{i=1}^{N} \left\langle Q_i^2 \right\rangle$, which we here call the "configuration scalar". Since the trace of the birefringence tensor **n** (or configuration tensor) is proportional to $\sum_{i=1}^{N} \left\langle Q_i^2 \right\rangle$, and $\text{trace}(\vec{\tau})$ is a function of $\sum_{i=1}^{N} \left\langle Q_i^2 \right\rangle$, there is a functional relationship between $\text{trace}(\vec{\tau})$ and $\text{trace}(\vec{n})$ which holds in any deformation history. Since, in strong extensional flows, the extensional stress is dominated by a single stress component and hence converges towards $\text{trace}(\vec{\tau})$, this choice for the dependence of the spring constant on normal modes implies that there is a roughly a one-to-one functional relationship between extensional stress and the conformation scalar, or birefringence. Hence one should expect little hysteresis from the FENE-PM model, as indeed shown to be the case in Figure 19. The large hysteresis predicted by the FENE-mode model thus arises from two sources: 1) the exclusion of modes other than the first two from the estimation of the spring constant, and 2) the re-weighting (or normalization) of the contributions of these two modes relative to that used in the FENE-PM model so that the spring constant in both the singly-folded and the fully folded highly stretched states are correctly calculated for these extreme configurations. These extreme conformations evidently dominate both stress and birefringence when the molecule is locally highly stretched, and when the molecule is not highly stretched locally, the FENE factor is near unity, and so approximations to it matter do not matter much. This physical insight used in the development of the FENE-mode model is evidently so successful that it not only out-performs the FENE-PM

model, but also the much more expensive multi-mode FENE-P model in the challenging test of the stress-conformation hysteresis. (Note that the multimode FENE-P model consists of N^2 equations, and so, for any given algorithm, is a factor of N slower than either the FENE-mode or FENE-PM models.)

In Fig. 20, we compare the predictions of the FENE-PM and the multimode FENE-P for varying ν with BD simulations, for the startup of shear flow (Wi = 100). Similar to the results for FENE-mode (Fig. 18), the predictions show systematically increasing deviation from BD simulation results at low strains, with decreasing number of modes. The single-mode FENE-PM converges to the multimode FENE-P model with one spring (equivalent to the FENE-P model), similar to the FENE-mode (Fig. 18). At high strains, the predictions agree well with one another. However, the locations of the stress overshoot for FENE-PM and multimode FENE-P models do not agree well with BD simulations, even for the finest resolution of the models.

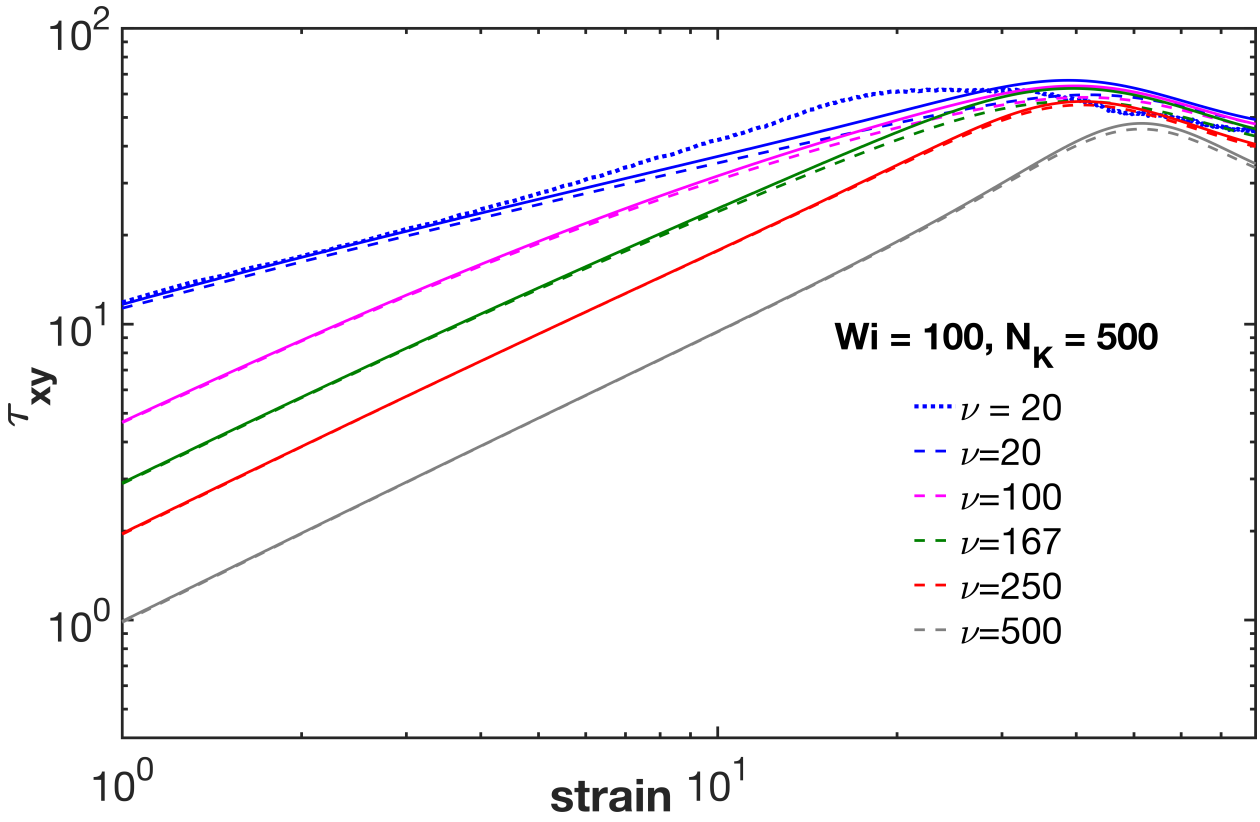

Figure 20: Same as Figure 18, except that the FENE-PM and the multimode FENE-P predictions (for varying ν) are shown by dashed and solid lines, respectively. Lines of same colour correspond to the same ν for both models.

Further, in Figures 21 and 22, we compare the predictions of the first normal stress difference and shear stress, respectively, for all the models – FENE-mode, FENE-PM and multimode FENE-P, for startup shear with flow reversal, for two different flow rates (Wi = 30 and 100). Overall, qualitative trends are similar across all models. However, the predictions of the FENE-mode model are in better agreement with the BD results than for the other models. In particular, the location of the shear stress overshoot for Wi = 100 in Figure 22 is well predicted by the FENE-mode model, whereas a delayed overshoot is observed for both the FENE-PM and the multimode FENE-P models. All three models under-predict the stress before the overshoot.

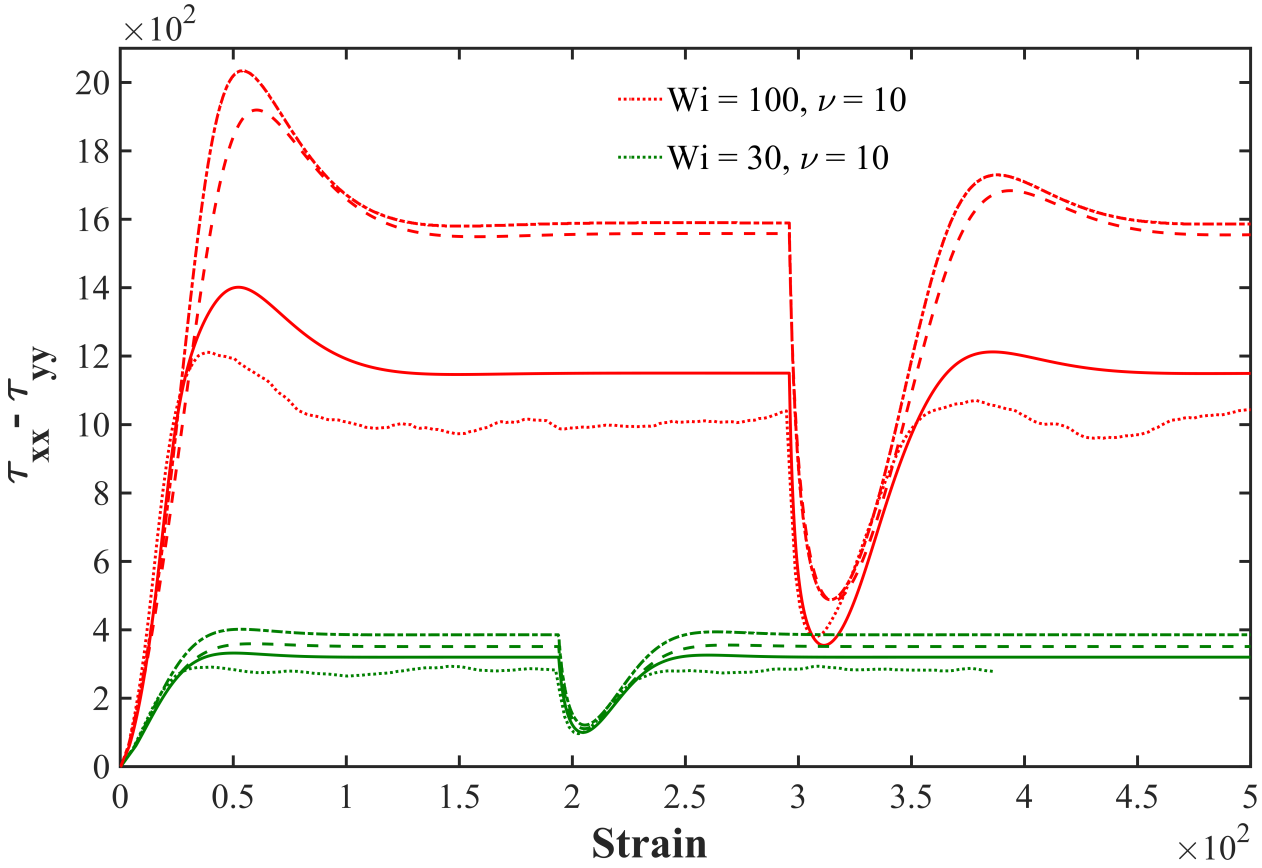

Figure 21: Time variation of the first normal stress difference for shear flows of Wi = 30 and 100, where the direction of the flow is reversed after several strains. The results from the BD simulations (N_K = 500) are shown by dotted lines, FENE-mode by solid lines, FENE-PM by dashed lines and multimode FENE-P by dash-dot lines. The results of Wi = 30 and 100 are shown in green and red colours, respectively. The BD simulation results are averaged over 2000 cases.

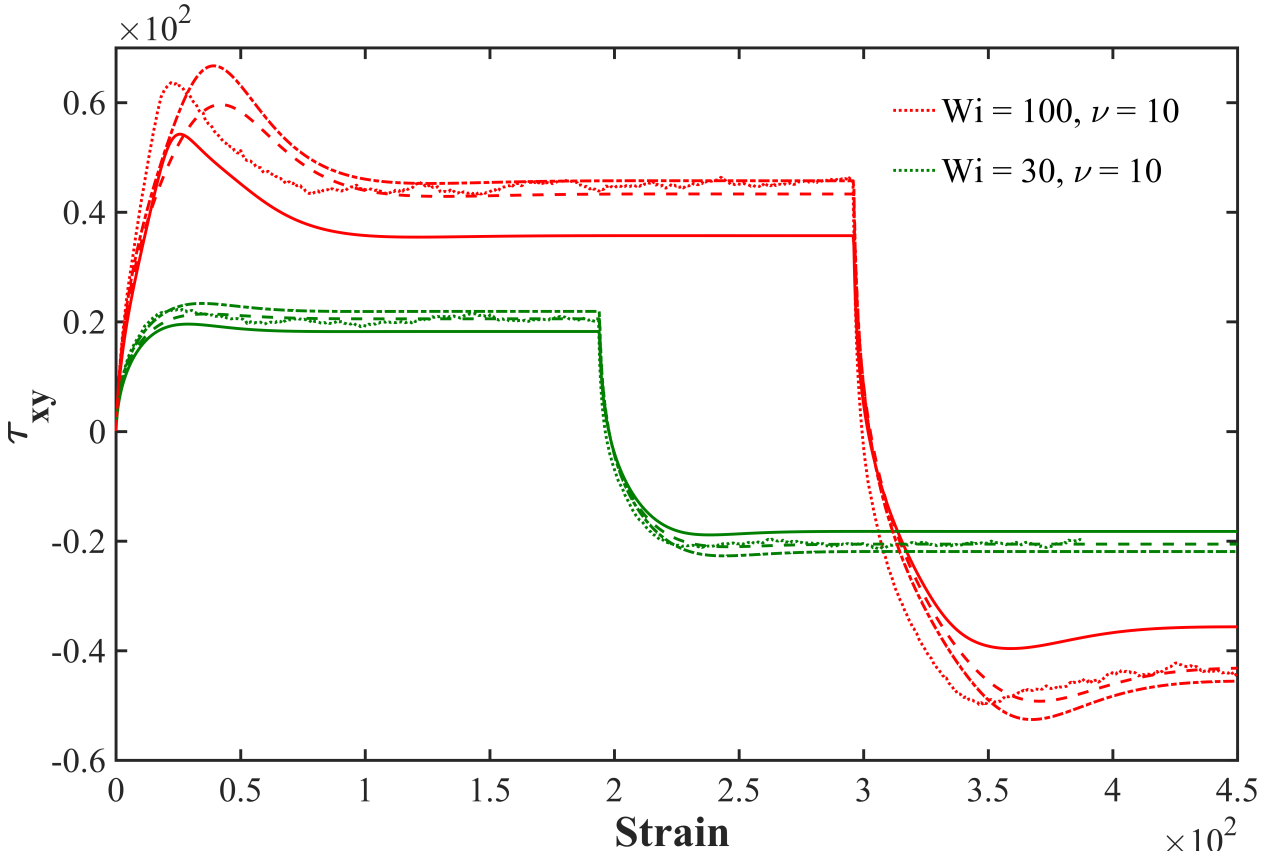

Figure 22: Same as Figure 21, except for the shear stress.

Thus, from the preceding discussion, it is clear that the FENE-mode model, even with two modes, provides predictions that agree much better with BD simulations than do those of the FENE-P model. The FENE-mode predictions are also a clear improvement to those of both the FENE-PM and the multimode FENE-P models, for the same number of modes. Hence, a two-mode FENE-mode model can possibly provide a cheap, but significant, enhancement over the FENE-P, which has been incorporated into various CFD packages. Finally, we note for each of the results presented in Fig. 15, a MATLAB code for the FENE-P calculations took approximately 0.1 seconds, using a single core of a 2.9 GHz Intel core i5 processor on a Macbook Pro laptop (early 2015 model). On the same laptop, a MATLAB code for the FENE-mode model took about 1.0-1.5 seconds to reproduce any of the results in Fig. 15. Note that while this execution time is more than 10 times

longer than for the FENE-P model, the computations are done for 25-50 modes for the FENE-mode model, when ν is taken to be 10-20, as in Fig. 15. In contrast, one BD simulation in uniaxial extension takes about one hour on a single core of an Intel Xeon processor (8, core, 16 threads in total; released in 2014) and about 30 minutes on a single core of an AMD Ryzen processor (8 core, 16 threads; released in 2018). Hence, on the same i5 processor that we used for testing the FENE-mode and FENE-P models, one single BD simulation will take much more than an hour to be executed. In addition, as mentioned in our figure captions, we have averaged over an ensemble of several hundred simulations to obtain good averages of stress in BD simulations. Thus, there is a difference in computational time of about 5-6 orders of magnitudes between the FENE-mode and the corresponding BD simulations. The FENE-mode model, on the other hand, is only an order of magnitude slower than the FENE-P model, while giving results much closer to the BD simulations. Furthermore, the cost of the FENE-mode calculations is roughly proportional to the number of modes used, and so can be brought down even closer to that of the (one-mode) FENE-P model, by trading accuracy for speed, at the discretion of the user. This opens the door to the use of the FENE-mode model in multi-dimensional polymer processing simulations, where the speed-accuracy trade-off is of acute importance. The ability to improve accuracy as desired will enable selective testing of numerical simulations for accuracy for limited special cases, and for optimization of error/cost with respect to both mesh refinement and model refinement, where the latter is carried out through changing the number of modes. In the future, the FENE-mode model might also be applied to the "stretch relaxation equation" in a tube model of entangled polymers, which would improve the accuracy of those models in fast flows, with limited increase in cost. The approach might also be extended to dilute solutions that include the effects of with

hydrodynamics interaction and/or excluded volume, by using methods pioneered by Öttinger [37] and by Prabhakar and Prakash [32].

Summary:

We have developed a new closed-form constitutive model, the "FENE-mode" model, to predict the time-dependent polymer conformation and stress of dilute polymer chains in solution more accurately than do previous closed-form models. The FENE-mode model achieves accuracy in conformational variables and in stress that is usually well within 20% of that from Brownian dynamics simulations, at a vastly smaller computational load. The FENE-mode model uses pre-averaged equations for the evolution of the conformation modes along with a representative spring constant derived from the magnitudes of the first two modes. We observe that the simplest function of the first two modes is able to capture the transient behavior of polymer chains in a variety of flow fields, as demonstrated by comparison with BD simulations of bead-spring chains. The magnitude of the first mode captures the effect of the end-to-end vector of the whole chain, while the magnitude of the second mode captures the effect of a single fold near the center of the chain. Evidently these two modes largely capture the effect of local stretch of the chain. If the chain is nearly fully extended, the magnitude of the normalized first mode approaches unity, while if the chain is highly stretched locally, but folded near the center, the magnitude of the first mode is small but that of the second mode approaches unity. Thus, if either mode is near unity, the chain is *locally* highly stretched, even if it is folded, and the spring constant is therefore large. Higher modes are needed to describe more complex folding patterns, but these evidently have much less impact on the stress and on the overall conformation of the chain. This is evidently because the effect of finer scale chain structure on the spring constant, represented by these higher modes, is

relatively small compared to the effects of the first two modes. The model is thus able to capture both the conformational and the corresponding stress variations quite accurately for extensional, shear and planar mixed flows between extension and shear, and between shear and pure rotation.

Acknowledgement:

ISD expresses his gratitude to the IIT Kanpur initiation grant for new faculties and the HPC center at IIT Kanpur. RGL acknowledges support by the National Science Foundation under Grant No. 1707640. Any opinions, findings, and conclusions or recommendations expressed in this material are those of the authors and do not necessarily reflect the views of NSF.

Appendix A: FENE-mode Equations for Various Flow Fields

In this Appendix, we show the derivation of analytical difference equations for the evolution of the normal modes for various flow fields used in this study.

Extensional flow:

The dynamics of the p^{th} normal mode is given as [35]:

$$\frac{d\vec{X}_p}{dt} + \frac{k_p}{\zeta_p}\vec{X}_p - \hat{\kappa}\cdot\vec{X}_p = \frac{1}{\zeta_p}\vec{f}_p \qquad \text{(A1)}$$

Here, $\vec{f}_p$ is the random force as defined in chapter 4 of the text by Doi and Edwards [35].

In addition, $\hat{\kappa}$ is the transpose of the gradient of the velocity. For uniaxial extensional flow, we have

$$\hat{\boldsymbol{\kappa}} = \begin{bmatrix} \dot{\varepsilon} & 0 & 0 \\ 0 & -\dot{\varepsilon}/2 & 0 \\ 0 & 0 & -\dot{\varepsilon}/2 \end{bmatrix} \tag{A2}$$

where $\dot{\varepsilon}$ is the extension rate. Then, from Eq. (A1), we obtain the following equation for the x-component (direction of stretching) of the normal mode *p*:

$$\frac{\mathrm{dX_{px}}}{\mathrm{dt}} + \left(\frac{k_p}{\zeta_p} - \dot{\varepsilon} \right) \mathrm{X_{px}} = \frac{1}{\zeta_p} f_{\mathrm{px}} \tag{A3}$$

Integrating for a small time increment from t to $t + \Delta t$, we get the following:

$$\mathrm{X_{px}}\left(t+\Delta t\right) = \mathrm{X_{px}}\left(t\right) e^{-\left[\left(k_p/\zeta_p\right)-\dot{\varepsilon}\right]\Delta t} + \int_t^{t+\Delta t} e^{-\left[\left(k_p/\zeta_p\right)-\dot{\varepsilon}\right]\left(t+\Delta t-\tau\right)} \frac{1}{\zeta_p} f_{px}\,\mathrm{d}\tau \tag{A4}$$

Using the definitions $E = \left[\left(k_p/\zeta_p\right) - \dot{\varepsilon}\right]$ and $\vec{f}'_{\mathrm{p}} = \frac{1}{\zeta_p}\vec{f}_{\mathrm{p}}$, Eq. (A4) becomes

$$\mathrm{X_{px}}\left(t+\Delta t\right) = \mathrm{X_{px}}\left(t\right) e^{-E\Delta t} + \int_t^{t+\Delta t} e^{-E\left(t+\Delta t-\tau\right)} f'_{px}\,\mathrm{d}\tau \tag{A5}$$

Using Eq. (A5), we can estimate the average of $\mathrm{X_{px}^2}\left(t+\Delta t\right)$ over all realizations:

$$\begin{aligned} \left\langle \mathrm{X_{px}^2}\left(t+\Delta t\right)\right\rangle &= \left\langle \mathrm{X_{px}^2}\left(t\right)\right\rangle e^{-2E\Delta t} + 2\int_t^{t+\Delta t} e^{-E\left(t+2\Delta t-\tau\right)} \left\langle \mathrm{X_{px}}\left(t\right) f'_{px}\left(\tau\right)\right\rangle \mathrm{d}\tau \\ &+ \int_t^{t+\Delta t} \mathrm{d}\tau' \int_t^{t+\Delta t} e^{-E\left(2t+2\Delta t-\tau-\tau'\right)} \left\langle f'_{px}\left(\tau'\right) f'_{px}\left(\tau\right)\right\rangle \mathrm{d}\tau \end{aligned} \tag{A6}$$

Note that this quantity can be obtained using Brownian dynamics simulations by averaging over multiple trajectories, each with a different initial starting state and each evolving due to a different Brownian noise history.

Using the fluctuation-dissipation theorem for the Brownian force correlations and the corresponding expression used in the Brownian dynamics simulations, we can simplify Eq. (A6) further to:

$$\left\langle \mathrm{X}_{\mathrm{px}}^2\left(t+\Delta t\right)\right\rangle = \left\langle \mathrm{X}_{\mathrm{px}}^2\left(t\right)\right\rangle e^{-2E\Delta t} + e^{-2E\left(t+\Delta t\right)}\frac{2\mathrm{k_B T}}{\zeta_p}\left[\frac{e^{2E\tau}}{2E}\right]_t^{t+\Delta t} \tag{A7}$$

Note that the second term on the RHS of Eq. (A6) vanishes due to a zero mean of the Brownian force over multiple realizations. The third term on the RHS in Eq. (A6) simplifies due to the fluctuation-dissipation theorem that says that the Brownian forces at different times are uncorrelated so that we finally arrive at the most simplified form:

$$\left\langle \mathrm{X}_{\mathrm{px}}^2\left(t+\Delta t\right)\right\rangle = \left\langle \mathrm{X}_{\mathrm{px}}^2\left(t\right)\right\rangle e^{-2E\Delta t} + \frac{\mathrm{k_B T}}{E\zeta_p}\left(1-e^{-2E\Delta t}\right) \tag{A8}$$

For a uniaxial extensional flow, the dynamics in the y- and z-directions are equivalent, so we only analyze the evolution in the y-direction here. The equation of motion of the p^{th} mode in the y-direction is given as:

$$\frac{\mathrm{dX_{py}}}{\mathrm{dt}} + \left(\frac{k_p}{\zeta_p} + \frac{\dot{\varepsilon}}{2}\right)\mathrm{X_{py}} = \frac{1}{\zeta_p} f_{\mathrm{py}} \tag{A9}$$

Using the definition $E' = \left[\left(k_p/\zeta_p\right) + \left(\dot{\varepsilon}/2\right)\right]$, we arrive at the final expression:

$$\left\langle \mathrm{X}_{\mathrm{py}}^2\left(t+\Delta t\right)\right\rangle = \left\langle \mathrm{X}_{\mathrm{py}}^2\left(t\right)\right\rangle e^{-2E'\Delta t} + \frac{\mathrm{k_B T}}{E'\zeta_p}\left(1-e^{-2E'\Delta t}\right) \tag{A10}$$

Shear flow:

For a simple steady shear flow, $\hat{\kappa}$ is given as:

$$\hat{\kappa} = \begin{bmatrix} 0 & \dot{\gamma} & 0 \\ 0 & 0 & 0 \\ 0 & 0 & 0 \end{bmatrix} \tag{A11}$$

where $\dot{\gamma}$ is the shear rate. The equation of motion of a mode in the y-direction is relatively simple for shear flow:

$$\frac{\mathrm{dX_{py}}}{\mathrm{dt}} + \frac{k_p}{\zeta_p}\mathrm{X_{py}} = \frac{1}{\zeta_p} f_{\mathrm{py}} \tag{A12}$$

Proceeding as for uniaxial extension, we can integrate this to obtain the following:

$$\mathrm{X_{py}}\left(t+\Delta t\right) = \mathrm{X_{py}}\left(t\right) e^{-\left(k_p/\zeta_p\right)\Delta t} + \int_t^{t+\Delta t} e^{-\left(k_p/\zeta_p\right)\left(t+\Delta t-\tau\right)} \frac{1}{\zeta_p} f_{py}\,\mathrm{d}\tau \tag{A13}$$

Then, we evaluate the average of the square of $\mathrm{X_{py}}\left(t+\Delta t\right)$ over all realizations, using similar arguments as before:

$$\left\langle \mathrm{X_{py}^2}\left(t+\Delta t\right)\right\rangle = \left\langle \mathrm{X_{py}^2}\left(t\right)\right\rangle e^{-2\left(k_p/\zeta_p\right)\Delta t} + \frac{\mathrm{k_B T}}{k_p}\left(1 - e^{-2\left(k_p/\zeta_p\right)\Delta t}\right) \tag{A14}$$

Next, we analyze the motion in the x-direction. The equation of motion is given as:

$$\frac{\mathrm{dX_{px}}}{\mathrm{dt}} = -\frac{k_p}{\zeta_p}\mathrm{X_{px}} + \left(\dot{\gamma}\mathrm{X_{py}} + \frac{1}{\zeta_p} f_{\mathrm{px}}\right) \tag{A15}$$

On integration, we arrive at:

$$\mathrm{X_{px}}\left(t+\Delta t\right) = \mathrm{X_{px}}\left(t\right) e^{-\left(k_p/\zeta_p\right)\Delta t} + \int_t^{t+\Delta t} e^{-\left(k_p/\zeta_p\right)\left(t+\Delta t-\tau\right)}\left(\dot{\gamma}\mathrm{X_{py}} + \frac{1}{\zeta_p} f_{px}\right)\mathrm{d}\tau \tag{A16}$$

Here, we are integrating within a vanishingly small time interval (i.e. between t and $t+\Delta t$). Thus, $\mathrm{X_{py}}$ can be approximately taken to be a constant for evaluating this integral. Thus, we get:

$$\mathrm{X_{px}}\left(t+\Delta t\right)=\mathrm{X_{px}}\left(t\right)e^{-\left(k_p/\zeta_p\right)\Delta t}+\dot{\gamma}\mathrm{X_{py}}e^{-\left(k_p/\zeta_p\right)\left(t+\Delta t\right)}\left[\frac{e^{\left(k_p/\zeta_p\right)\tau}}{\left(k_p/\zeta_p\right)}\right]_t^{t+\Delta t}+\int_t^{t+\Delta t}e^{-\left(k_p/\zeta_p\right)\left(t+\Delta t-\tau\right)}\frac{1}{\zeta_p}f_{px}\mathrm{d}\tau \quad \text{(A17)}$$

Further simplifying yields

$$\mathrm{X_{px}}\left(t+\Delta t\right)=\mathrm{X_{px}}\left(t\right)e^{-\left(k_p/\zeta_p\right)\Delta t}+\dot{\gamma}\mathrm{X_{py}}\frac{\zeta_p}{k_p}\left(1-e^{-\left(k_p/\zeta_p\right)\Delta t}\right)+\int_t^{t+\Delta t}e^{-\left(k_p/\zeta_p\right)\left(t+\Delta t-\tau\right)}\frac{1}{\zeta_p}f_{px}\mathrm{d}\tau \quad \text{(A18)}$$

Squaring of this gives:

$$\begin{aligned}\mathrm{X_{px}^2}\left(t+\Delta t\right)&=\mathrm{X_{px}^2}\left(t\right)e^{-\left(2k_p/\zeta_p\right)\Delta t}+\dot{\gamma}^2\mathrm{X_{py}^2}\left(t\right)\frac{\zeta_p^2}{k_p^2}\left(1-e^{-\left(k_p/\zeta_p\right)\Delta t}\right)^2+2\mathrm{X_{px}}\left(t\right)e^{-\left(k_p/\zeta_p\right)\Delta t}\dot{\gamma}\mathrm{X_{py}}\left(t\right)\frac{\zeta_p}{k_p}\left(1-e^{-\left(k_p/\zeta_p\right)\Delta t}\right)\\&+2\int_t^{t+\Delta t}e^{-\left(k_p/\zeta_p\right)\left(t+2\Delta t-\tau\right)}\frac{1}{\zeta_p}f_{px}\mathrm{X_{px}}\mathrm{d}\tau+2\int_t^{t+\Delta t}e^{-\left(k_p/\zeta_p\right)\left(t+\Delta t-\tau\right)}\frac{1}{\zeta_p}f_{px}\mathrm{X_{px}}\dot{\gamma}\mathrm{X_{py}}\left(t\right)\frac{\zeta_p}{k_p}\left(1-e^{-\left(k_p/\zeta_p\right)\Delta t}\right)\mathrm{d}\tau\\&+\int_t^{t+\Delta t}\mathrm{d}\tau'\int_t^{t+\Delta t}e^{-\left(k_p/\zeta_p\right)\left(2t+2\Delta t-\tau-\tau'\right)}\frac{1}{\zeta_p^2}f_{px}\left(\tau\right)f_{px}\left(\tau'\right)\mathrm{d}\tau\end{aligned} \quad \text{(A19)}$$

Now, we proceed as before to take the average of the square over all realizations. Then, after further simplifications, we arrive at the following final expression:

$$\begin{aligned}\left\langle\mathrm{X_{px}^2}\left(t+\Delta t\right)\right\rangle&=\left\langle\mathrm{X_{px}^2}\left(t\right)\right\rangle e^{-\left(2k_p/\zeta_p\right)\Delta t}+\dot{\gamma}^2\left\langle\mathrm{X_{py}^2}\left(t\right)\right\rangle\frac{\zeta_p^2}{k_p^2}\left(1-e^{-\left(k_p/\zeta_p\right)\Delta t}\right)^2\\&+2\left\langle\mathrm{X_{px}X_{py}}\left(t\right)\right\rangle\dot{\gamma}\frac{\zeta_p}{k_p}\left(e^{-\left(k_p/\zeta_p\right)\Delta t}-e^{-2\left(k_p/\zeta_p\right)\Delta t}\right)+\frac{\mathrm{k_B T}}{k_p}\left(1-e^{-\left(2k_p/\zeta_p\right)\Delta t}\right)\end{aligned} \quad \text{(A20)}$$

Note that, an expression for $\left\langle\mathrm{X_{px}X_{py}}\left(t\right)\right\rangle$ can be derived using Eqs. (A13) and (A18), followed by further simplifications:

$$\left\langle\mathrm{X_{px}X_{py}}\left(t+\Delta t\right)\right\rangle=\left\langle\mathrm{X_{px}X_{py}}\left(t\right)\right\rangle e^{-2\left(k_p/\zeta_p\right)\Delta t}+\dot{\gamma}\left\langle\mathrm{X_{py}^2}\left(t\right)\right\rangle\frac{\zeta_p}{k_p}\left(e^{-\left(k_p/\zeta_p\right)\Delta t}-e^{-2\left(k_p/\zeta_p\right)\Delta t}\right) \quad \text{(A21)}$$

Planar mixed flows:

Apart from uniaxial extensional and shear flows, we also perform BD simulations for planar flows in between extensional and shear flows, and between shear and purely rotational flows. For a general planar mixed flow, $\hat{\kappa}$ is given as:

$$\hat{\kappa} = \begin{bmatrix} 0 & \dot{\gamma} & 0 \\ \alpha\dot{\gamma} & 0 & 0 \\ 0 & 0 & 0 \end{bmatrix} \tag{A22}$$

where the parameter α can assume values from -1 to 1 and controls the character of the flow. For such a mixed flow, we arrive at the following equations of motion for the normal modes in the x- and y-directions, respectively:

$$\frac{\mathrm{dX_{px}}}{\mathrm{dt}} + \left(\frac{k_p}{\zeta_p} \mathrm{X_{px}} - \dot{\gamma} \mathrm{X_{py}} \right) = \frac{1}{\zeta_p} f_{\mathrm{px}} \tag{A23}$$

$$\frac{\mathrm{dX_{py}}}{\mathrm{dt}} + \left(\frac{k_p}{\zeta_p} \mathrm{X_{py}} - \alpha\dot{\gamma} \mathrm{X_{px}} \right) = \frac{1}{\zeta_p} f_{\mathrm{py}} \tag{A24}$$

Integrating Eqs. (A23) and (A24) over a small time interval, as before, we obtain the following:

$$\mathrm{X_{px}}\left(t+\Delta t\right) = \mathrm{X_{px}}\left(t\right) e^{-\left(k_p/\zeta_p\right)\Delta t} + \dot{\gamma} \mathrm{X_{py}} \frac{\zeta_p}{k_p} \left(1 - e^{-\left(k_p/\zeta_p\right)\Delta t}\right) + \int_t^{t+\Delta t} e^{-\left(k_p/\zeta_p\right)\left(t+\Delta t-\tau\right)} \frac{1}{\zeta_p} f_{px} \mathrm{d}\tau \tag{A25}$$

$$\mathrm{X_{py}}\left(t+\Delta t\right) = \mathrm{X_{py}}\left(t\right) e^{-\left(k_p/\zeta_p\right)\Delta t} + \alpha\dot{\gamma} \mathrm{X_{px}} \frac{\zeta_p}{k_p} \left(1 - e^{-\left(k_p/\zeta_p\right)\Delta t}\right) + \int_t^{t+\Delta t} e^{-\left(k_p/\zeta_p\right)\left(t+\Delta t-\tau\right)} \frac{1}{\zeta_p} f_{py} \mathrm{d}\tau \tag{A26}$$

Then, the evolution of the average of the square of these quantities, over multiple realizations, is given as:

$$\begin{aligned} \left\langle \mathrm{X_{px}^2}\left(t+\Delta t\right) \right\rangle &= \left\langle \mathrm{X_{px}^2}\left(t\right) \right\rangle e^{-\left(2k_p/\zeta_p\right)\Delta t} + \dot{\gamma}^2 \left\langle \mathrm{X_{py}^2}\left(t\right) \right\rangle \frac{\zeta_p^2}{k_p^2} \left(1 - e^{-\left(k_p/\zeta_p\right)\Delta t}\right)^2 \\ &+ 2\left\langle \mathrm{X_{px}X_{py}}\left(t\right) \right\rangle \dot{\gamma} \frac{\zeta_p}{k_p} \left(e^{-\left(k_p/\zeta_p\right)\Delta t} - e^{-2\left(k_p/\zeta_p\right)\Delta t} \right) + \frac{\mathrm{k_B T}}{k_p} \left(1 - e^{-\left(2k_p/\zeta_p\right)\Delta t}\right) \end{aligned} \tag{A27}$$

$$\left\langle \mathrm{X}_{\mathrm{py}}^2\left(t+\Delta t\right)\right\rangle = \left\langle \mathrm{X}_{\mathrm{py}}^2\left(t\right)\right\rangle e^{-\left(2k_p/\zeta_p\right)\Delta t} + \alpha^2\dot{\gamma}^2\left\langle \mathrm{X}_{\mathrm{px}}^2\left(t\right)\right\rangle \frac{\zeta_p^2}{k_p^2}\left(1-e^{-\left(k_p/\zeta_p\right)\Delta t}\right)^2$$
$$+2\left\langle \mathrm{X}_{\mathrm{px}}\mathrm{X}_{\mathrm{py}}\left(t\right)\right\rangle \alpha\dot{\gamma}\frac{\zeta_p}{k_p}\left(e^{-\left(k_p/\zeta_p\right)\Delta t}-e^{-2\left(k_p/\zeta_p\right)\Delta t}\right)+\frac{\mathrm{k_B T}}{k_p}\left(1-e^{-\left(2k_p/\zeta_p\right)\Delta t}\right) \tag{A28}$$

To arrive at these simplified equations, we have used the same arguments as before. Using Eqs. (A25) and (A26), we can get a simplified expression for $\left\langle \mathrm{X}_{\mathrm{px}}\mathrm{X}_{\mathrm{py}}\left(t\right)\right\rangle$:

$$\left\langle \mathrm{X}_{\mathrm{px}}\mathrm{X}_{\mathrm{py}}\left(t+\Delta t\right)\right\rangle = \left\langle \mathrm{X}_{\mathrm{px}}\mathrm{X}_{\mathrm{py}}\left(t\right)\right\rangle e^{-2\left(k_p/\zeta_p\right)\Delta t} + \alpha\dot{\gamma}\left\langle \mathrm{X}_{\mathrm{px}}^2\left(t\right)\right\rangle \frac{\zeta_p}{k_p}\left(e^{-\left(k_p/\zeta_p\right)\Delta t}-e^{-2\left(k_p/\zeta_p\right)\Delta t}\right)$$
$$+\dot{\gamma}\left\langle \mathrm{X}_{\mathrm{py}}^2\left(t\right)\right\rangle \frac{\zeta_p}{k_p}\left(e^{-\left(k_p/\zeta_p\right)\Delta t}-e^{-2\left(k_p/\zeta_p\right)\Delta t}\right)+\alpha\dot{\gamma}^2\left\langle \mathrm{X}_{\mathrm{px}}\mathrm{X}_{\mathrm{py}}\left(t\right)\right\rangle \frac{\zeta_p^2}{k_p^2}\left(1-e^{-\left(k_p/\zeta_p\right)\Delta t}\right)^2 \tag{A29}$$

Appendix B: Virtual Work and Derivation of the Stress Tensor

In bead-spring models, the stress tensor is derivable from the principle of virtual work, which assures that simulations involving any deformation history will always result in non-decreasing entropy, so that the second law of thermodynamics is satisfied. Under this principle, the elastic work required to deform the polymer is given by the change in free energy, which must be a state variable that depends only the "state" of the system and not the path to get to that state. The rate of doing work when the stress tensor is symmetric, is

$$\dot{W} = \vec{\vec{\tau}} : \vec{\vec{D}} \tag{B1}$$

where $\vec{\vec{D}}$ is the rate of strain tensor, or the symmetrized velocity gradient tensor, $\vec{\vec{D}} = \frac{1}{2}\left(\hat{\kappa}+\hat{\kappa}^T\right)$.

To apply the virtual work argument, one takes the deformation to be ideally fast enough to leave no time for chain relaxation that would dissipate energy. Under these conditions, the work *W* must be a state variable, independent of the history of deformation and only dependent on state

quantities. Microscopically, the proper state variables are the elastic energy stored in the individual springs, and for the linear Rouse model, one can show that W is just the sum of elastic energy in all springs. However, for pre-averaged models, information about individual springs is lost, and one must be content with using other, appropriate, state variables. The most obvious of these are invariants of the stress tensor, and for the simple Rouse model, the elastic free energy is just one half the trace of the stress tensor, i.e., $W = \frac{1}{2} tr\left(\vec{\vec{\tau}}\right)$. When the spring is nonlinear and closure approximations are used, to be safe, one needs a corresponding formula for the free energy. For a multi-spring or multi-mode model, where the total stress is the sum of contributions from each spring, or from each mode, one might show that each spring, or each mode, satisfies a modal version of Eq. (B1) with W_i depending only on a state variable, for spring i or mode i, which is typically the trace of the partial stress tensor for that spring or mode. A weaker, but satisfactory, satisfaction of this principle is to show that the sum of stress contributions from all springs, or from all modes, satisfies Eq. (B1), using a state variable for the entire chain, typically the trace of the overall stress tensor.

As we discuss below, the multi-spring FENE-P model and the multi-mode FENE-PM model both satisfy the principle of virtual work under all deformation histories, and are for that reason thermodynamically "safe." We will show here that our new, FENE-mode, model does not satisfy this principle under all conditions, but appears to satisfy it in two different limits, namely the limit in which the springs are only modestly stretched and therefore remain Hookean, and in the highly stretched limit, where the springs are nearly completely stretched. We first discuss the conventional virtual work argument applied to FENE-P, FENE-PM and FENE-mode models, and

then show how to apply an appropriate version of it to the FENE-mode model at high spring stretch.

Conventional virtual work argument and pre-averaged FENE models

For FENE-P type models, under a fast deformation with negligible relaxation term, the constitutive equation can be written in terms of "conformational tensor" for each mode, such as $\left\langle \vec{Q}_i \vec{Q}_i \right\rangle$ for each spring *i*, or $\vec{\vec{S}}_p \equiv \frac{2p^2\pi^2}{N}\left\langle \vec{X}_p \vec{X}_p \right\rangle$, for each mode. Under fast flows, with negligible relaxation, the dynamical equation for these has the form:

$$\overset{\nabla}{\vec{\vec{S}}} \equiv \frac{d}{dt}\vec{\vec{S}}_p - \hat{\kappa}\cdot\vec{\vec{S}}_p - \vec{\vec{S}}_p\cdot\hat{\kappa}^T = 0 \qquad \text{(B2)}$$

Where $\overset{\nabla}{\vec{\vec{S}}}$ is the upper-convected derivative of $\vec{\vec{S}}_p$. An equivalent equation applies to the tensor $\left\langle \vec{Q}_i \vec{Q}_i \right\rangle$. Taking the trace of Eq. (B2) gives

$$\frac{d}{dt} tr\left(\vec{\vec{S}}_p\right) = \vec{\vec{S}}_p : \vec{\vec{D}} \qquad \text{(B3)}$$

Thus, the rate of doing work associated with mode *p* is given by multiplying each side of Eq. (B3) by the pre-averaged spring constant for mode *p*, k_p:

$$k_p \frac{d}{dt} tr\left(\vec{\vec{S}}_p\right) = k_p \vec{\vec{S}}_p : \vec{\vec{D}} = \vec{\vec{\tau}}_p : \vec{\vec{D}} = \dot{W}_p \qquad \text{(B4)}$$

where the modal stress $\vec{\vec{\tau}}_p$ is taken as the product of its spring constant k_p and the mode conformation tensor $\vec{\vec{S}}_p$. If k_p is a function of $tr\left(\vec{\vec{S}}_p\right)$ only, then W_p is a function $tr\left(\vec{\vec{S}}_p\right)$ only, and therefore is a function of a state variable. The total stress then is also a function of all the state

variables, which are the $tr\left(\vec{\vec{S}}_p\right)$ values. The same argument applies to expressions written in terms of spring conformation tensors $\left\langle \vec{Q}_i\vec{Q}_i \right\rangle$, with k_i a function of $tr\left\langle \vec{Q}_i\vec{Q}_i \right\rangle$. In both cases, the total work, which is sum of the partial work functions W_p or W_i, is a function of the set of state variables, one for each mode. This guarantees that the stress tensor satisfies a virtual work argument with work a function of state variables only, and not deformation history.

For the multimode FENE-P model [39], the stress is a sum over contributions $k_i\left\langle \vec{Q}_i\vec{Q}_i \right\rangle$ from each spring, where each k_i is a function only of $tr\left\langle \vec{Q}_i\vec{Q}_i \right\rangle$ and so this model satisfies the virtual work argument. For the FENE-PM model [38], written in terms of modes, the spring constant is the same for all modes, and is a function of $\sum_p tr\left(\vec{\vec{S}}_p\right)$; which is equal to $\sum_i tr\left\langle \vec{Q}_i\vec{Q}_i \right\rangle$. Thus, $\sum_p tr\left(\vec{\vec{S}}_p\right)$ is the state variable, upon which the total work W depends by integrating

$$\dot{W} = \vec{\vec{\tau}} : \vec{\vec{D}} = k\sum_p \vec{\vec{S}}_p : \vec{\vec{D}} = k\frac{d}{dt}\sum_p tr\left(\vec{\vec{S}}_p\right) \tag{B5}$$

where we have used Eq. (B3) to obtain the final expression. Since the spring constant k is a function of $\sum_p tr\left(\vec{\vec{S}}_p\right)$ we can integrate Eq. (B5), to obtain the total free energy W as a function of the state variable $\sum_p tr\left(\vec{\vec{S}}_p\right)$. This means that the stress tensor for the FENE-PM model satisfies the virtual work principle with work a function of a state variable.

Now, our FENE-mode model uses a modal representation and we have taken our stress tensor to be given by $\vec{\vec{\tau}}_p = k\vec{\vec{S}}_p$, where the spring constant k is the same for each mode, but k is a function

of the trace of the first two modes only, $tr\left(\vec{\vec{S}}_1\right)$ and $tr\left(\vec{\vec{S}}_2\right)$. This means that we cannot in general write a differential equation to obtain a partial work W_p for each mode separately, because the equation for mode p depends on the trace of at least one other modal variable. Neither can we write a differential equation for the total work W, since the spring constant does not depend only on the sum $\sum_p tr\left(\vec{\vec{S}}_p\right)$. Nevertheless, our constitutive equation predicts stress remarkably well for all the deformation histories we have considered, including ones with reversing strain history, and with relaxation. We believe that the reason for this success is that the FENE-mode model trivially satisfies the virtual work argument in the limit of modest strains and also seems to satisfy it when the chain is highly stretched in a folded or fully extended state, as we now show.

Virtual work argument for the FENE-mode spring constant for highly deformed chains:

In FENE-mode, it is assumed that all springs in the chain are equally stretched, to a value l_{sp}. Now, to obtain the spring constant, we have to calculate the fractional extension $\hat{r} = \frac{l_{sp}}{\nu b_K}$, which is shown to be

$$\hat{r} = \frac{1}{2}\left(\frac{\bar{X}_2}{\bar{X}_{2\max}}\right) + \sqrt{\left(\frac{1}{2}\frac{\bar{X}_2}{\bar{X}_{2\max}} + \frac{\bar{X}_1}{\bar{X}_{1\max}}\right)^2 - \left(\frac{\bar{X}_2}{\bar{X}_{2\max}}\right)\left(\frac{\bar{X}_1}{\bar{X}_{1\max}}\right)} \qquad \text{(B6)}$$

where the simple addition formula $\frac{\bar{X}_2}{\bar{X}_{2\max}} + \frac{\bar{X}_1}{\bar{X}_{1\max}}$ in Eq. (18) of the two modes is just an approximation of this general expression. However, since all springs are equally stretched, we have $\sqrt{tr\left(\vec{Q}_i\vec{Q}_i\right)} = l_{sp}$ for any i. This means that $\sum_i tr\left(\vec{Q}_i\vec{Q}_i\right) = Nl_{sp}^2$. Thus, we have

$$\frac{\bar{X}_2}{\bar{X}_{2\max}}+\frac{\bar{X}_1}{\bar{X}_{1\max}}\approx\frac{1}{2}\left(\frac{\bar{X}_2}{\bar{X}_{2\max}}\right)+\sqrt{\left(\frac{1}{2}\frac{\bar{X}_2}{\bar{X}_{2\max}}+\frac{\bar{X}_1}{\bar{X}_{1\max}}\right)^2-\left(\frac{\bar{X}_2}{\bar{X}_{2\max}}\right)\left(\frac{\bar{X}_1}{\bar{X}_{1\max}}\right)}=\hat{r}=\frac{\sqrt{\sum_i tr\left(\vec{Q}_i\vec{Q}_i\right)}}{\sqrt{N}\nu b_K} \quad \text{(B7)}$$

So, the sum of these two modal variables in the form we are using in the FENE-mode model is indeed a function of $\sum_i tr\left(\vec{Q}_i\vec{Q}_i\right)$ in this limit, which is also equal to the sum of the traces of the normal modes $\sum_p tr\left(\vec{\vec{S}}_p\right)$. Also, note that the spring constant for the FENE-mode model is a function of $\hat{r}^2$. Thus, Eq. (B5) applies to this situation, and *W* can be obtained by an integral over the state variable $\sum_p tr\left(\vec{\vec{S}}_p\right)$. Hence, there is a free energy function from which our formula for the stress can be derived by the virtual work argument. We note here that for the high stretch limit considered here, since the spring constant approaches infinity as the inverse of the difference between $\sum_p tr\left(\vec{\vec{S}}_p\right)$ and its maximum value, the free energy *W* will depend logarithmically on this difference and thus will approach infinity as the stretch approaches its maximum value, similar to the behavior of the simple FENE-P dumbbell. Thus, our stress formula is valid for both modest and very high stresses. That it works so well over the whole range of conditions studied is surprising, but at least can be rationalized by its accuracy in the two limits. The closure of the multi-mode FENE-P model uses spring constants that are functions of the individual springs only while the spring constant for the FENE-PM model is a function of only the entire chain configuration, and thus both closures lack the strong dependence of the spring constants on both the first and second mode in the limit of the folded chain with most individual springs highly stretched. While our stress tensor in this limit is technically an "elastic" stress, this stress relaxes so rapidly when straining stops that it can be considered virtually dissipative. The ability to capture

this nearly dissipative limit before the chain is fully unraveled is likely at the heart of the success of the FENE-mode model, especially in capturing the stress-conformation hysteresis.

Our FENE-mode model in the highly stretched limit thus encapsulates insights generated by the "kink dynamics" simulations of Larson [36], wherein a folded chain that is nearly fully stretched locally, unravels under deformation, with stress being essentially dissipative, as solvent flows past inextensible chain segments. Thus, the innovation in the FENE-mode model is to recognize that the nonlinearity of the spring is most needed when spring deformation is severe, and in flows that produce such deformations, folded states occur which can be accounted for using a spring constant that is a function of a simple linear combination of the two slowest modes.

References

[1] Smith, D. E.; Babcock, H. P.; Chu, S. Single-Polymer Dynamics in Steady Shear Flow. *Science* **1999**, *283,* 1724-1727.

[2] Perkins, T. T.; Smith, D. E.; Chu, S. Single Polymer Dynamics in an Elongational Flow. *Science* **1997**, *276*, 2016-2021.

[3] Schroeder, C. M.; Babcock, H. P.; Shaqfeh, E. S. G.; Chu, S. Observation of Polymer Conformation Hysteresis in Extensional Flow. *Science* **2003***, 301*, 1515-1519.

[4] Smith, D. E.; Chu, S. Response of Flexible Polymers to a Sudden Elongational Flow. *Science* **1998***, 281*, 1335-1340.

[5] Lee, E. C.; Solomon, M. J.; Muller, S. J. Molecular Orientation and Deformation of Polymer Solutions under Shear: A Flow Light Scattering Study. *Macromolecules* **1997**, *30*, 7313-7321.

[6] Lee, E. C.; Muller, S. J. Flow light scattering studies of polymer coil conformation in solutions under shear: effect of solvent quality. *Polymer* **1999**, *40*, 2501-2510.

[7] Hur, J. S.; Shaqfeh, E. S. G.; Babcock, H. P.; Smith, D. E.; Chu, S. Dynamics of dilute and semidilute DNA solutions in the start-up of shear flow. *Journal of Rheology* **2001**, *45*, 421.

[8] Schroeder, C. M.; Teixeira, R. E.; Shaqfeh, E. S. G.; Chu, S. Characteristic Periodic Motion of Polymers in Shear Flow. *Physical Review Letters* **2005**, *95*, 018301.

[9] Link, A.; Springer, J. Light Scattering from Dilute Polymer Solutions in Shear Flow. *Macromolecules* **1993**, *26*, 464-471.

[10] Bossart, J.; Öttinger, H. C. Orientation of Polymer Coils in Dilute Solutions Undergoing Shear Flow: Birefringence and Light Scattering. *Macromolecules* **1995**, *28*, 5852-5860.

[11] Bossart, J.; Öttinger, H. C. Orientation of Polymer Coils in Dilute Solutions Undergoing Shear Flow: Birefringence Experiments. *Macromolecules* **1997**, *30*, 5527-5540.

[12] Rouse, P. R. A Theory of the Linear Viscoelastic Properties of Dilute Solutions of Coiling Polymers. *Journal of Chemical Physics* **1953**, *21*, 1272.

[13] Zimm, B. H. Dynamics of Polymer Molecules in Dilute Solution: Viscoelasticity, Flow Birefringence and Dielectric Loss. *Journal of Chemical Physics* **1956**, *24*, 269.

[14] Liu, T. W. Flexible polymer chain dynamics and rheological properties in steady flows. *Journal of Chemical Physics* **1989**, *90*, 5826.

[15] Doyle, P.; Shaqfeh, E. S. G.; Gast, A. P. Dynamic simulation of freely draining flexible polymers in steady linear flows. *Journal of Fluid Mechanics* **1997**, *334*, 251-291.

[16] Petera, D.; Muthukumar, M. Brownian dynamics simulation of bead–rod chains under shear with hydrodynamic interaction. *Journal of Chemical Physics* **1999**, *111*, 7614.

[17] Hur, J. S.; Shaqfeh, E. S. G.; Larson, R. G. Brownian dynamics simulations of single DNA molecules in shear flow. *Journal of Rheology* **2000**, *44*, 713.

[18] Hsieh, C. C.; Larson, R. G. Modeling hydrodynamic interaction in Brownian dynamics: Simulations of extensional and shear flows of dilute solutions of high molecular weight polystyrene. *Journal of Rheology* **2004**, *48*, 995.

[19] Hsieh, C. C.; Lei, L.; Larson, R. G. Modeling hydrodynamic interaction in Brownian dynamics: simulations of extensional flows of dilute solutions of DNA and polystyrene. *Journal of Non-Newtonian Fluid Mechanics* **2003**, *113*, 147-191.

[20] Lee, J. S.; Shaqfeh, E. S. G.; Muller, S. J. Dynamics of DNA tumbling in shear to rotational mixed flows: Pathways and periods. *Physical Review E* **2007**, *75*, 040802.

[21] Larson, R. G.; Hu, H.; Smith, D. E.; Chu, S. Brownian dynamics simulations of a DNA molecule in an extensional flow field. *Journal of Rheology* **1999**, *43*, 267.

[22] Hsieh, C. C.; Larson, R. G. Prediction of coil-stretch hysteresis for dilute polystyrene molecules in extensional flow. *Journal of Rheology* **2005**, *49*, 1081.

[23] Sendner, C.; Netz, R. R. Single flexible and semiflexible polymers at high shear: Non-monotonic and non-universal stretching response. *The European Physical Journal E* **2009**, *30*, 75-81.

[24] Saha Dalal, I.; Hoda, N.; Larson, R. G. Multiple regimes of deformation in shearing flow of isolated polymers. *Journal of Rheology* **2012**, *56*, 305.

[25] Saha Dalal, I.; Albaugh, A.; Hoda, N.; Larson, R. G. Tumbling and Deformation of Isolated Polymer Chains in Shearing Flow. *Macromolecules* **2012**, *45*, 9493-9499.

[26] Saha Dalal, I.; Hsieh, C. C.; Albaugh, A.; Larson, R. G. Effects of excluded volume and hydrodynamic interactions on the behavior of isolated bead-rod polymer chains in shearing flow. *AIChE Journal* **2014**, *60*, 1400-1412.

[27] Saha Dalal, I.; Larson, R. G. Explaining the Absence of High-Frequency Viscoelastic Relaxation Modes of Polymers in Dilute Solutions. *Macromolecules* **2013**, *46*, 1981-1992.

[28] Larson, R. G. The rheology of dilute solutions of flexible polymers: Progress and problems. *Journal of Rheology* **2005**, *49*, 1.

[29] van der Brule, B. H. A. A. Browian dynamics simulation of finitely extensible bead - spring chains. *Journal of Non-Newtonian Fluid Mechanics* **1993**, *47*, 357-378.

[30] Ghosh, I.; Joo, Y. L.; McKinley, G. H.; Brown, R. A.; Armstrong, R. C. A new model for dilute polymer solutions in flows with strong extensional components. *Journal of Rheology* **2002**, *46* (5), 1057-1089.

[31] Wedgewood, L. E.; Öttinger, H. C. A model of dilute polymer solutions with hydrodynamic interaction and finite extensibility. II. Shear flows. *Journal of non-Newtonian Fluid Mechanics* **1988**, *27*, 245-264.

[32] Prabhakar, R.; Ravi Prakash, J. Gaussian approximation for finitely extensible bead-spring chains with hydrodynamic interaction. *Journal of Rheology* **2006**, *50*, 561-593.

[33] Bird, R. B.; Dotson, P. J.; Johnson, N. L. Polymer solution rheology based on a finitely extensible bead—spring chain model. *Journal of Non-Newtonian Fluid Mechanics* **1980**, *7*, 213-235.

[34] Dealy, J. M.; Read, D. J.; Larson, R. G. *Structure and Rheology of Molten Polymers, From Structure to Flow Behavior and Back Again*; Carl Hanser Verlag GmbH & Co., 2018.

[35] Doi, M.; Edwards, S. F. *The Theory of Polymer Dynamics*; Oxford University Press, 1986.

[36] Larson, R. G. The unraveling of a polymer chain in a strong extensional flow. *Rheologica Acta* **1990**, *29*, 371-384.

[37] Öttinger, H. C. Gaussian approximation for Rouse chains with hydrodynamic interaction. *Journal of Chemical Physics* **1989**, *90*, 463-473.

[38] Wedgewood, L. E.; Ostrov, D. N.; Byron Bird, R. A finitely extensible bead-spring chain model for dilute polymer solutions. *Journal of Non-Newtonian Fluid Mechanics* **1991**, *40*, 119-139.

[39] Wiest, J. M.; Wedgewood, L. E.; Byron Bird, R. On coil–stretch transitions in dilute polymer solutions. *Journal of Chemical Physics* **1989**, *90*, 587-594.

[40] Doyle, P.; Shaqfeh, E. S. G.; McKinley, Gareth H.; Spiegelberg, S. H. Relaxation of dilute polymer solutions following extensional flow. *Journal of Non-Newtonian Fluid Mechanics* **1998**, *76*, 79-110.

[41] Shaqfeh, E. S. G. The dynamics of single-molecule DNA in flows. *Journal of Non-Newtonian Fluid Mechanics* **2005**, *130*, 1-28.

[42] Schroeder, C. M. Single Polymer Dynamics for Molecular Rheology. *Journal of Rheology* **2018**, *62*, 371–403.

[43] Prakash, J. R. Universal dynamics of dilute and semidilute solutions of flexible linear polymers. *Current Opinion in Colloid & Interface Science* **2019**, *43*, 63–79.

[44] Saadat, A.; Khomami, B. Molecular based prediction of the extensional rheology of high molecular weight polystyrene dilute solutions: A hi-fidelity Brownian dynamics approach. *Journal of Rheology* **2015**, *59*, 1507-1525.

[45] Saadat, A.; Khomami, B. Letter to the Editor: BDpack, an open source parallel Brownian dynamics simulation package. *Journal of Rheology* **2016**, *61*, 147-149.

[46] Jain, A.; Sasmal, C.; Hartkamp, R.; Todd, B. D.; Prakash, J. R. Brownian dynamics simulations of planar mixed flows of polymer solutions at finite concentrations. *Chem. Eng. Sci.* **2015**, 121, 245–257.

[47] Wagner, C. E.; McKinley, G. H. The importance of flow history in mixed shear and extensional flows. *Journal of Non-Newtonian Fluid Mechanics* **2016**, *233*, 133–145.

[48] Kishbaugh, A. J.; McHugh, A. J. A discussion of shear-thickening in bead-spring models. *Journal of Non-Newtonian Fluid Mechanics* **1990**, *34*, 181-206.

[49] Herrchen, M.; Öttinger, H. C. A detailed comparison of various FENE dumbbell models. *Journal of Non-Newtonian Fluid Mechanics* **1997**, *68*, 17-42.

[50] Lielens, G.; Keunings, R.; Legat, V. The FENE-L and FENE-LS closure approximations to the kinetic theory of finitely extensible dumbbells. *Journal of Non-Newtonian Fluid Mechanics* **1999**, *87*, 179-196.